ADVANCED BIOLOGY
www.advanced-bio.com

# Astrocytes in Paper Chips and Their Interaction with Hybrid Vesicles

*Cathrine Abild Meyer, Paula De Dios Andres, Edit Brodszkij, Isabella N. Westensee, Joseph Lyons, Sandra H. Vaz,* and Brigitte Städler**

**The role of astrocytes in brain function has received increased attention lately due to their critical role in brain development and function under physiological and pathophysiological conditions. However, the biological evaluation of soft material nanoparticles in astrocytes remains unexplored. Here, the interaction of crosslinked hybrid vesicles (HVs) and either C8-D1A astrocytes or primary astrocytes cultured in polystyrene tissue culture or floatable paper-based chips is investigated. The amphiphilic block copolymer poly(cholesteryl methacrylate)-*block*-poly(2-carboxyethyl acrylate) (P1) and 1,2-dioleoyl-*sn*-glycero-3-phosphoethanolamine lipids are used for the assembly of HVs with crosslinked membranes. The assemblies show no short-term toxicity towards the C8-D1A astrocytes and the primary astrocytes, and both cell types internalize the HVs when cultured in 2D cell culture. Further, it is demonstrated that both the C8-D1A astrocytes and the primary astrocytes could mature in paper-based chips with preserved calcium signaling and glial fibrillary acidic protein expression. Last, it is confirmed that both types of astrocytes could internalize the HVs when cultured in paper-based chips. These findings lay out a fundamental understanding of the interaction between soft material nanoparticles and astrocytes, even when primary astrocytes are cultured in paper-based chips offering a 3D environment.**

## 1. Introduction

The role of astrocytes in brain function has received a surge in interest due to their relevant activity for brain homeostasis and responsiveness to neurotransmitters.[1] Among other functions, astrocytes are responsible for the maintenance of glutamate homeostasis by supporting its synthesis, uptake, and release via the glutamate-glutamine cycle. In addition, they are the main effectors of glycolysis in order to produce lactate that is delivered to neurons through the astrocyte-neuron lactate shuttle.[2] Astrocytes are able to control synaptic function since they sense the neurotransmitter release by neurons, responding with increased calcium levels and release of gliotransmitters that will control synaptic transmission and plasticity.[3] Moreover, astrocytes participate in the blood–brain barrier (BBB) formation and maintenance, establishing the link between the endothelial blood flux and neurons.[4] Several studies indicated that astrocytic homeostatic failure occurs under pathophysiological condition, for example, in individuals affected by amyotrophic lateral sclerosis (ALS). The manipulation of astrocytes towards a physiological phenotype promotes the improvement of disease condition.[5] The role of dysfunctional astrocytes in the pathogenesis of ALS indicates that astrocytes may be targeted with strategies for their revival, and this strategies may include the use of nanomaterials.

Nanoformulations are a widely explored concept to administer therapeutic compounds to cells as extensively discussed in multiple recent reviews.[6] Surprisingly, the biological evaluation of soft material nanoparticles with astrocytes remains largely unexplored. Reports only started to emerge likely due to the fast increasing appreciation of the astrocytes' importance. For instance, endocytosed methylprednisolone-loaded carboxymethylchitosan/poly(amidoamine) dendrimer nanoparticles were evaluated in primary rat astrocytes.[7] The authors found that these nanoparticles could be retained for up to 7 days in the astrocytes, but they also observed an increase in the frequency of transient exocytotic fusion events. In a more recent example, Papa et al. illustrated that nanogels were internalized by primary rat astrocytes via the clathrin-mediated endocytosis being localized in the lysosomes.[8]

From a different perspective, polymer-lipid hybrid vesicles (HVs) are an alternative vesicular assembly to liposomes

C. Abild Meyer, P. De Dios Andres, E. Brodszkij, I. N. Westensee, J. Lyons, B. Städler
Interdisciplinary Nanoscience Center (iNANO)
Aarhus University
8000 Aarhus, Denmark
E-mail: bstadler@inano.au.dk
S. H. Vaz
Instituto de Medicina Molecular João Lobo Antunes
Faculdade de Medicina da Universidade de Lisboa
1649-028 Lisboa, Portugal
E-mail: svaz@medicina.ulisboa.pt
S. H. Vaz
Instituto de Farmacologia e Neurociências
Faculdade de Medicina da Universidade de Lisboa
1649-028 Lisboa, Portugal
The ORCID identification number(s) for the author(s) of this article can be found under https://doi.org/10.1002/adbi.202200209.



**DOI: 10.1002/adbi.202200209**

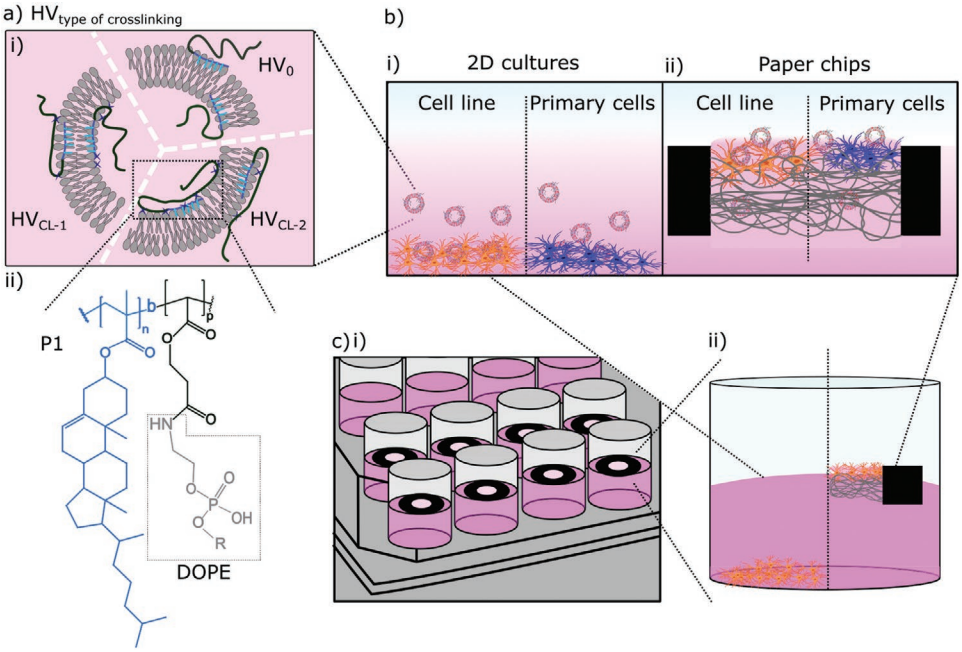


**Scheme 1.** a) i) Cartoon illustrating assembled hybrid vesicles (HVs) with different degrees of crosslinking (indicated by crosses). ii) HVs were assembled using poly(cholesteryl methacrylate)-*block*-poly(2-carboxyethyl acrylate) (P1) and 1,2-dioleoyl-*sn*-glycero-3-phosphoethanolamine (DOPE). The R indicates the hydrophobic part of the lipid. b) Primary astrocytes or C8-D1A cell line cultured in i) 2D cultures or ii) paper chips. c) i) Well plate showing floating paper chips and ii) an illustration of the two cell culture set-ups.

and polymersomes as discussed in more detail in several reviews.[9] HVs benefit from the excellent self-assembly ability of (phospho)lipids, and the design opportunities amphiphilic block copolymers offer. The stability of HVs toward disintegration can remain challenging. Crosslinking is a widely explored opportunity to stabilize soft material nanoparticles such as liposomes,[10] liposomes with a covalent polymer coating,[11] micelles,[12] or polymersomes.[13] However, crosslinking of the membrane building blocks in HVs remains unexplored.

Here, we explore the interaction of HVs with crosslinked membranes with either C8-D1A astrocytes or primary cultured astrocytes from rats, either as a 2D cell layer on tissue culture polystyrene or in the fibrous 3D environment of floating paper chips (**Scheme 1**). Specifically, we i) assembled and characterized HVs with crosslinked membranes using the amphiphilic block copolymer poly(cholesteryl methacrylate)-*block*- poly(2-carboxyethyl acrylate) (P1) and 1,2-dioleoyl-*sn*-glycero-3-phosphoethanolamine (DOPE) lipids, iii) evaluated short-term toxicity, the uptake efficacy and intracellular location of the HVs in 2D cell culture, iii) demonstrated that C8-D1A astrocytes or primary astrocytes could mature in floating paper chips with preserved calcium signalling ability and glial fibrillary acidic protein (GFAP) expression in the latter case, and iv) confirmed that the astrocytes cultured in the paper chips could internalize the HVs.

## 2. Results and Discussion

### 2.1. HVs Assembly

We chose 1,2-dioleoyl-*sn*-glycero-3-phosphoethanolamine (DOPE) as the lipid since we previously showed that DOPE could be used to assemble HVs,[14] and the amine group on the head group lends itself for covalent crosslinking with carboxyl groups. The amphiphilic block copolymer poly(cholesteryl methacrylate)-*block*-poly(2-carboxyethyl acrylate) (P1) was used as the polymeric part. P1 was previously successfully employed as building block in HVs assembly.[14,15] Importantly, the hydrophilic extension carries the required carboxyl groups for crosslinking with DOPE via *N*-3-(3-dimethylaminopropyl)carbodiimide hydrochloride/*N*-hydroxy succinimide (EDC/NHS) chemistry (Scheme 1).

The HVs were assembled via the rehydration method, crosslinked, and purified via size exclusion chromatography (SEC). (An overview over all the assembled HVs can be found in Table S1, Supporting Information). The level of crosslinking was controlled by varying the amount of EDC and NHS added to the HVs, resulting in $HV_{CL-1}$ and $HV_{CL-2}$ where $HV_{CL-2}$ was expected to have a membrane with a higher crosslinking degree. Non-crosslinked HVs are referred to as $HV_0$. Transmission electron microscopy (TEM) images showed spherical vesicles without a clear micellar population in all cases (**Figure 1**a). $HV_{CL-2}$ showed more particle-like morphology and higher structural integrity on the TEM grids compared to $HV_0$ and $HV_{CL-1}$, probably indicating crosslinking of the building blocks. Cryogenic electron microscopy (cryo-EM) images of $HV_{CL-2}$ confirmed the preserved vesicular appearance (Figure 1a, top image).

The hydrodynamic radius ($D_h$) obtained from dynamic light scattering (DLS) measurements decreased from ≈238 nm for $HV_0$ to ≈218 and ≈210 nm for $HV_{CL-1}$ and $HV_{CL-2}$, respectively, with comparably low polydispersity indexes (PDI) suggesting that the crosslinking step changed the vesicles' membrane, that is, the crosslinking step pulled the building blocks

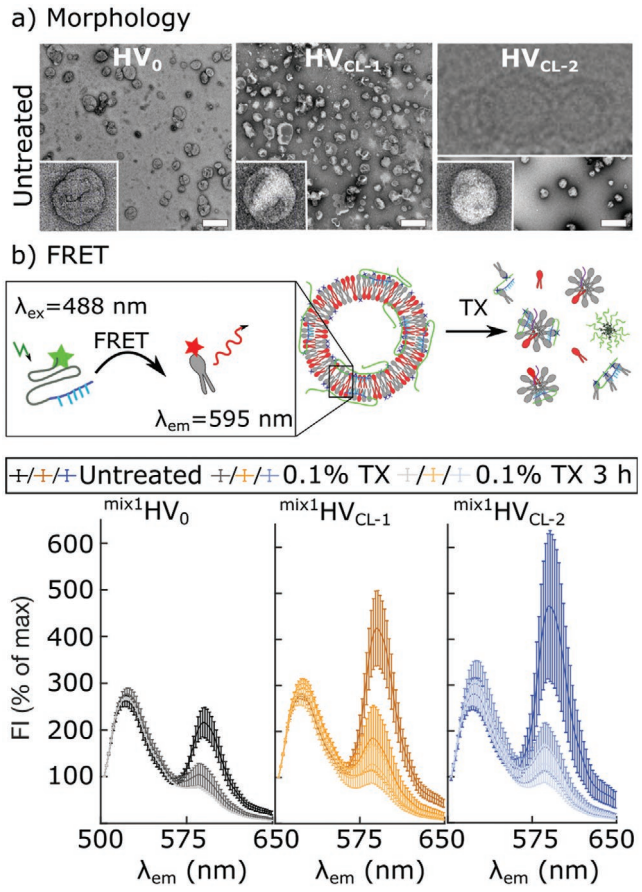


**Figure 1.** HV assembly: a) Representative TEM images of $HV_0$, $HV_{CL-1}$, and $HV_{CL-2}$ including a cryo-EM image of $HV_{CL-2}$. Scale bars are 500 nm. b) Schematic of HVs showing energy transfer from $P1^{OG}$ to $^{Rho}PE$. Normalized fluorescent emission spectra of $^{mix1}HV_0$, $^{mix1}HV_{CL-1}$, and $^{mix1}HV_{CL-2}$ before (darkest color) and after exposure to 0.1% TX immediately and after 3 h. The data are expressed as normalized mean ± SD ($n = 3$).

closer resulting in smaller vesicles (Table S2 and Figure S1, Supporting Information). In addition, we used Oregon green-labeled P1 ($P1^{OG}$) and 1,2-dimyristoyl-*sn*-glycero-3-phosphoethanolamine-*N*-(lissamine rhodamine B sulfonyl) ($^{Rho}PE$) during the assembly resulting in $^{mix1}HV_0$, $^{mix1}HV_{CL-1}$, and $^{mix1}HV_{CL-2}$ because these two fluorophores can act as a fluorescence resonance energy transfer (FRET) pair. FRET is an interesting method to confirm the presence of hybrid membranes since only fluorophores in close proximity can transfer energy. The samples were excited at $\lambda_{ex} = 488$ nm and the emission spectra were recorded from $\lambda_{em} = 503$–$650$ nm. All three types of HVs showed a FRET effect, but the FRET efficiency increased with increasing crosslinking density, that is, the FRET efficiencies were 42%, 57%, and 59% for $^{mix1}HV_0$, $^{mix1}HV_{CL-1}$, and $^{mix1}HV_{CL-2}$, respectively, illustrating that the crosslinking of the building blocks likely put more of the fluorophores in close proximity for energy transfer (Figure 1c). Further, the initial FRET efficiency was compared to the FRET efficiency after the exposure to Triton X-100 (TX). The emission peak originating from $P1^{OG}$ ($\lambda_{em} = 526$ nm) slightly increased and emission peak originating from $^{Rho}PE$ ($\lambda_{em} = 583$ nm) decreased and shifted to lower wavelength when the different HVs were incubated with TX. The FRET efficiencies were ≈27%, ≈37%, and ≈34% for fluorescent emission spectra of $^{mix1}HV_0$, $^{mix1}HV_{CL-1}$, and $^{mix1}HV_{CL-2}$, respectively, and substantially lower compared to the HVs prior to TX exposure. It should be noted that $^{Rho}PE$ was not crosslinked with the polymeric building blocks since the amine at the head group was used for fluorophore conjugation, that is, the presence of TX likely separated the non-crosslinked building blocks, and no conclusions on the stability of the vesicles could be drawn based on these FRET experiments. Therefore, we assembled HVs using rhodamine-labeled P1 ($P1^{Rho}$) and 1,2-dipalmitoyl-*sn*-glycero-3-phosphoethanolamine-*N*-(7-nitro-2-1,3-benzoxadiazol-4-yl) ($^{NBD}PE$). The latter was a tail-labeled lipid that could be crosslinked with P1 resulting in $^{mix2}HV_0$, $^{mix2}HV_{CL-1}$, and $^{mix2}HV_{CL-2}$. The emission spectra of these assemblies ($\lambda_{ex}$ = 488 nm) showed a dominating emission peak originating from $^{NBD}PE$, while the emission peak for $P1^{Rho}$ was only slightly visible for $^{mix2}HV_{CL-2}$ (Figure S2ai, Supporting Information). This observation was a combination of the broad emission peak of $^{NBD}PE$ and the generally low signal from $P1^{Rho}$ likely due to low polymer labeling efficiency (Figure S2aii, Supporting Information). Therefore, the FRET efficiencies could not be reliably calculated.

Complementary, the stability of $HV_0$, $HV_{CL-1}$, and $HV_{CL-2}$ was assessed by recording correlograms before and after exposure to 0.02% TX using DLS (**Figure 2**a). The correlograms of $HV_0$ showed the expected disintegration of the vesicle following TX exposure. On the other hand, $HV_{CL-1}$ and $HV_{CL-2}$ had only small changes in their correlograms following TX exposure, suggesting their superior stability due to the crosslinking. In addition, TEM images of $HV_0$ confirmed their disintegration upon exposure to TX, while the morphologies of $HV_{CL-1}$ and $HV_{CL-2}$ seemed retained (Figure 2a, insets). Cryo-EM images of $HV_{CL-2}$ revealed that the initially unilamellar vesicles became multilamellar after exposure to TX (Figure 2a, inset bottom image). We speculate that the interaction with TX led to the expected swelling due to surfactant molecule incorporation but the subsequent micellization step could not occur due to the crosslinked building block. Consequently, the unilamellar membrane might have split into multiple lamellae to reduce unfavorable transmembrane imbalances.

The morphological changes in the HVs were assessed using DLS when the environmental pH was lowered to pH 4 and cycled back to pH 7.4. This experiment was a simplistic mimic of the conditions the HVs are expected to experience in the lysosomes/endosomes when internalized by mammalian cells via endocytosis. The recorded correlograms showed shifting to longer times, that is, increase in size and PDI when the pH was lowered to 4, in all cases. Additionally, no recovery was observed when the pH was increased back to 7.4, suggesting irreversible structural changes in the assemblies that could not be prevented by crosslinking the DOPE and P1 (Figure S2b, Supporting Information).

The membrane packing of the HVs is an important aspect that affects their stability and permeability. We used the environmental sensitive probe Laurdan to assess differences in membrane fluidity of $HV_0$, $HV_{CL-1}$, and $HV_{CL-2}$. The calculated general polarization (GP) was ≈0.05 and independent on the type of HVs, but in agreement with our previously published

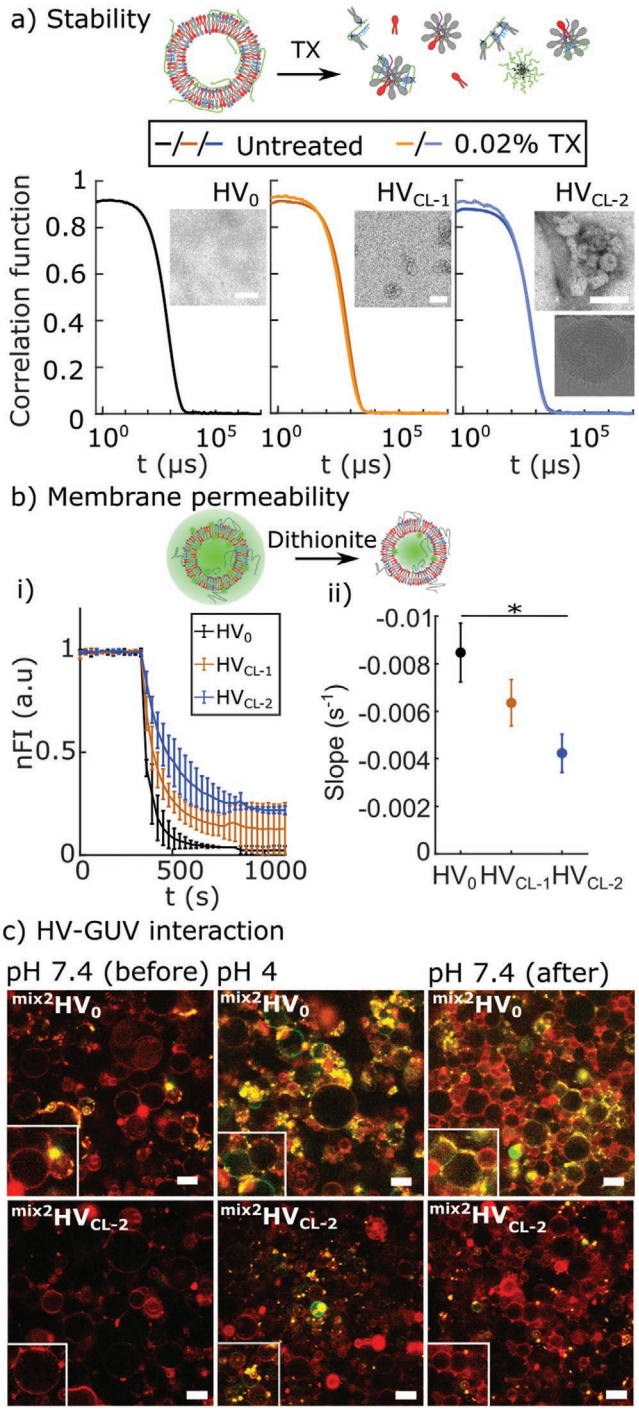


**Figure 2.** HV characterization: a) Correlograms obtained from DLS of $HV_0$, $HV_{CL-1}$, and $HV_{CL-2}$ before and after exposure to 0.02% TX including TEM images of the samples and a cryo-EM image of $HV_{CL-2}$ after TX treatment (bottom right image ($n = 1$). Scale bars are 200 µm. b) i) Time dependent normalized fluorescent intensity (nFI) of $^{NBD}$PE labeled $HV_0$, $HV_{CL-1}$, and $HV_{CL-2}$ when exposed to dithionite. The data are expressed as normalized mean ± SD ($n = 3$). ii) Slopes of the linear decay of nFI from the dithionite-based quenching assay. ($n = 3$, $^*p < 0.05$; one-way ANOVA with Turkey's multiple comparison test; data expressed as normalized mean ± SD). c) Representative CLSM images of $^{mix2}HV_{CL-2}$ and $^{mix2}HV_0$ interacting with unlabeled GUVs at pH 7.4, at pH 4, and when the pH was returned to pH 7.4 (green: $^{NBD}$PE; red: $P1^{Rho}$; $n = 2$). Scale bars are 10 µm.

results[14] that indicated stiffer membranes when DOPE was used instead of 1,2-Dioleoyl-sn-glycero-3-phosphocholine (DOPC) (Figure S2c, Supporting Information). These results suggested that the membrane packing was predominantly controlled by the used lipids, and that the crosslinking likely only affected the membrane on the surface.

With the aim to evaluate the effect of the crosslinking on the membrane permeability, we incubated $HV_0$, $HV_{CL-1}$, and $HV_{CL-2}$, which all contained $^{NBD}$PE, with a final concentration of 2 mM dithionite and the fluorescent intensity decrease was measured over time (Figure 2bi). Dithionite salt irreversible quenches the NBD dye and can therefore be used to study the permeability of the membranes by following the degree of fluorescent intensity decrease when dithionite is added. Ideally, only 50% of the NBD should be quenched if the membrane is not permeable to dithionite and spontaneous transmembrane lipid flipping is excluded. Here, all HVs had higher quenching values, which meant that they had some degree of dithionite permeability. Nonetheless, the fluorescence intensity decay showed differences depending on the crosslinking degree of the HVs, that is, increased crosslinking density of the HVs resulted in slower fluorescence decay and plateauing at higher values, suggesting that less dithionite was able to cross the membrane. In other words, the slopes of the initial decay showed significant differences between $HV_0$ and $HV_{CL-2}$, confirming differences in permeability of the different membranes (Figure 2bii).

Finally, we assessed the interaction of $^{mix2}HV_0$, $^{mix2}HV_{CL-1}$, and $^{mix2}HV_{CL-2}$ with a model membrane in the form of (unlabeled) giant unilamellar vesicles (GUVs) made of DOPC lipids (Figure 2c and Figure S3, Supporting Information). Confocal laser scanning microscopy (CLSM) images of GUVs mixed with $^{mix2}HV_0$ at pH 7.4 showed fluorescent signals originating from both $P1^{Rho}$ and $^{NBD}$PE, suggesting that both building blocks of $^{mix2}HV_0$ incorporated into the membrane of the GUVs. In contrast, CLSM images of GUVs mixed with $^{mix2}HV_{CL-1}$ and $^{mix2}HV_{CL-2}$ at pH 7.4 presented predominantly a fluorescent signal originating from $P1^{Rho}$, indicating that mostly the polymer incorporated in their membrane. When the pH was lowered to 4, GUVs mixed with $^{mix2}HV_0$ showed a patchy fluorescent signal originating from both $P1^{Rho}$ and $^{NBD}$PE, suggesting an inhomogeneous incorporation of $P1^{Rho}$ and $^{NBD}$PE in the GUVs' membrane. It should be noted that the incorporation at pH 4 was more efficient than at pH 7.4 likely due to the loss in amphiphilic nature of the $P1^{Rho}$ when the carboxyl groups became protonated. Further, few GUVs mixed with $^{mix2}HV_{CL-1}$ had a patchy fluorescent signal that seemed to rather be originating from aggregated $^{mix2}HV_{CL-1}$ on the surface of the GUVs than from membrane incorporation of the building blocks, suggesting that even the less efficiently crosslinked vesicles improved their stability. When the pH was increased back to pH 7.4, the GUVs mixed with $^{mix2}HV_0$ and $^{mix2}HV_{CL-1}$ were smaller in size and aggregated, pointing toward an irreversible interaction. In contrast, almost no fluorescent signal originating from $^{NBD}$PE was detectable in GUVs mixed with $^{mix2}HV_{CL-2}$ at pH 4 and almost no changes were observed when the pH was returned to 7.4, suggesting a crosslinking related improved stability of $^{mix2}HV_{CL-2}$.

### 2.2. HV Interaction with Astrocytes

#### *2.2.1. C8-D1A Astrocytes Cell Line*

With the aim to conduct a basic biological evaluation, the short-term cytotoxicity and the uptake efficacy of the HVs were assessed using the C8-D1A astrocyte cell line cultured in standard tissue-culture polystyrene 96-well plates. First, the absence of inherent short-term toxicity of $HV_0$, $HV_{CL-1}$, and $HV_{CL-2}$ when incubated with C8-D1A astrocyte for 24 h was confirmed (**Figure 3**a). Second, the association of $^{mix1}HV_0$, $^{mix1}HV_{CL-1}$, and $^{mix1}HV_{CL-2}$ with C8-D1A astrocytes within 24 h was monitored by flow cytometry in the green channel ($\lambda_{em}$ = 495–555 nm, read-out for $P1^{OG}$) and the yellow channel ($\lambda_{em}$ = 557–609 nm, read-out for $^{Rho}PE$) using an excitation wavelength of $\lambda_{ex}$ = 488 nm to follow the fate of $P1^{OG}$ and $^{Rho}PE$, respectively. The histograms showed a shift to higher fluorescent intensities in both channels over time indicating an increased uptake of the HVs. Further, it was revealed that the uptake of HVs split up the C8-D1A astrocytes in two populations: one showing positive cells with a high association with HVs and one showing very low/no association (Figure 3bi). More specifically, the number

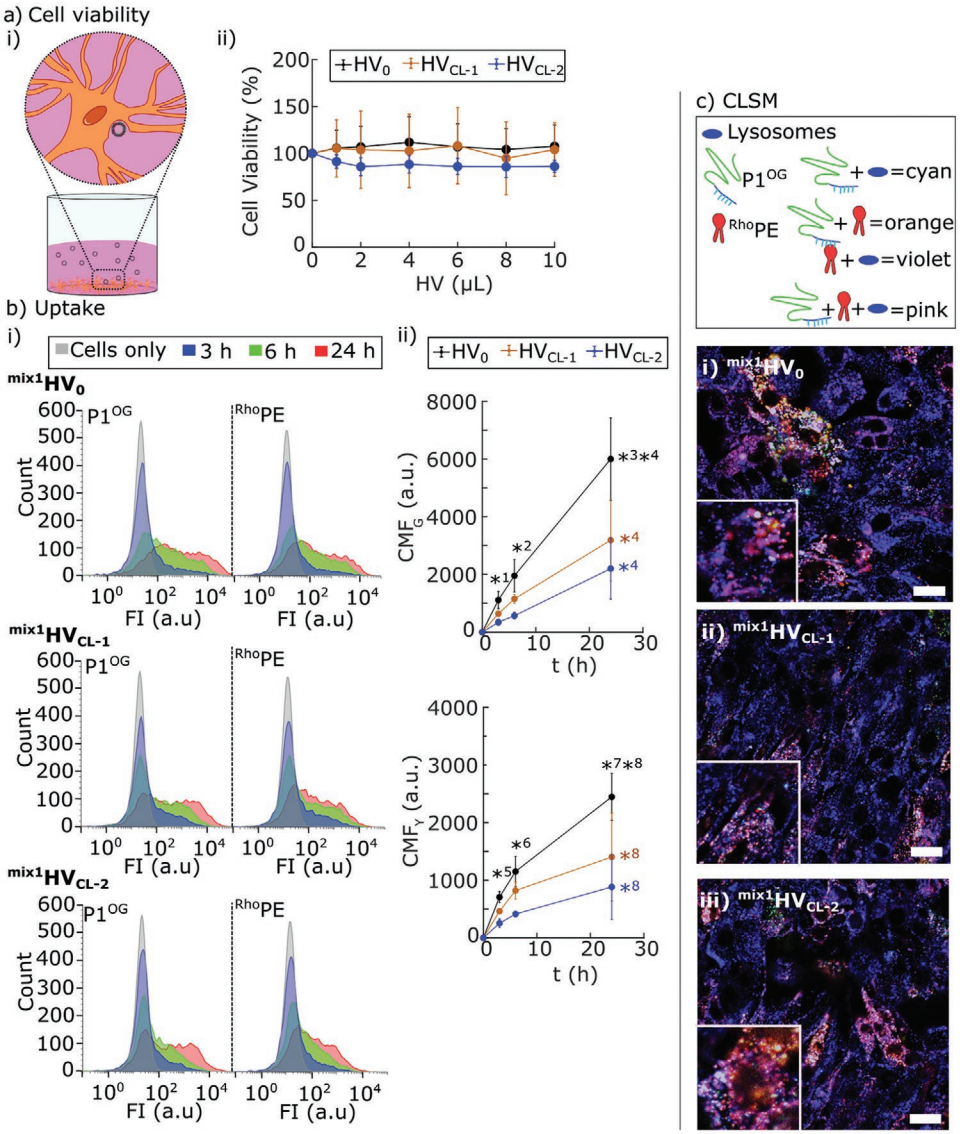


**Figure 3.** C8-D1A astrocyte cell line–HV interaction in 2D culture: a) i) Cartoon showing interaction of C8-D1A astrocytes with HVs. ii) Short-term viability of C8-D1A astrocytes exposed to $HV_0$, $HV_{CL-1}$, and $HV_{CL-2}$ for 24 h. The data are expressed as mean ± SD ($n$ = 3). b) i) Representative histograms obtained by flow cytometry of cells incubated with $^{mix1}HV_0$, $^{mix1}HV_{CL-1}$, and $^{mix1}HV_{CL-2}$ for 24 h ($n$ = 3). ii) Cell mean fluorescence (CMF) of C8-D1A astrocytes after exposure to $^{mix1}HV_0$, $^{mix1}HV_{CL-1}$, and $^{mix1}HV_{CL-2}$ for 3, 6, and 24 h ($P1^{OG}$: green channel; $^{Rho}PE$: yellow channel; $n$ = 3, $*p < 0.05$: comparing in the green channel: 1) $^{mix1}HV_0$ at 3 h compared to $^{mix1}HV_{CL-1}$ and $^{mix1}HV_{CL-2}$ at 3 h, 2) $^{mix1}HV_0$ at 6 h compared to $^{mix1}HV_{CL-2}$ at 6 h, 3) $^{mix1}HV_0$ at 24 h compared to $^{mix1}HV_{CL-2}$ at 24 h, 4) All samples at 24 h compared to 0, 3, and 6 h within the same sample; comparing in the yellow channel, 5) all samples compared to each other at 3 h, 6) $^{mix1}HV_0$ at 6 h compared to $^{mix1}HV_{CL-2}$ at 6 h, 7) $^{mix1}HV_0$ at 24 h compared to $^{mix1}HV_{CL-2}$ at 24 h, 8) all samples at 24 h compared to 0 and 3 h within the same sample. The data are expressed as mean ± SD. c) Representative CLSM images of cells incubated with $^{mix1}HV_0$, $^{mix1}HV_{CL-1}$, and $^{mix1}HV_{CL-2}$ for 24 h (blue: LysoTracker deep Red stained lysosomes; green: $P1^{OG}$; red: $^{Rho}PE$). Scale bars are 20 µm ($n$ = 2).

of positive cells (i.e., cells associated with the HVs) increased over time reaching >80% within 24 h independent on the type of HVs (Figure S4a, Supporting Information). However, there was a trend that less positive cells were detected after 3 h incubation with $^{mix1}HV_{CL-2}$ compared to incubation with $^{mix1}HV_0$, probably due to the lower amount of charged group available on the surface of $^{mix1}HV_{CL-2}$, since they were used for crosslinking.

Next, the cell mean fluorescence (CMF) in the positive cells was monitored over time in the green and yellow channel (Figure 3bii). In general, the CMF for C8-D1A astrocytes increased within the 24 h when incubated with the different types of HVs. However, the CMF was statistically significantly higher when the cells were incubated with $^{mix1}HV_0$ compared to $^{mix1}HV_{CL-2}$ at all measured time points and in both channels. The CMF of the C8-D1A astrocytes exposed to $^{mix1}HV_{CL-1}$ was lower and higher compared to cells incubated with $^{mix1}HV_0$ and $^{mix1}HV_{CL-2,}$ respectively, but without statistical significance. We attributed this finding again to the fact that the crosslinking step lowered the amount of charged groups on the surface of the HVs.

Complementary, the C8-D1A cells with stained lysosomes were visualized by CLSM after incubation with $^{mix1}HV_0$, $^{mix1}HV_{CL-1}$, and $^{mix1}HV_{CL-2}$ for 24 h (Figure 3c). The images showed that all types of HVs were internalized by the C8-D1A cells. However, the level of internalization within the same cell population for the same HVs varied greatly, that is, ≈30% of the cells showed high levels of HVs internalization, while the rest had barely any fluorescent signal that would indicate the presence of the HVs. These are substantially fewer cells compared to the flow cytometry results, probably due to the better statistics and higher sensitivity of the latter technique. There is only limited literature on nanoparticle internalization by astrocytes available, and a detailed investigation on this unexpected finding will be part of a future publication.

### 2.2.2. Primary Astrocytes

Complementary, the interaction of the HVs was evaluated in a more realistic setting using primary cortical astrocytes prepared from 0–2 days old Wistar pups, and that were used after 14 days in vitro (DIV). First, the absence of short-term toxicity of $HV_0$, $HV_{CL-1}$, and $HV_{CL-2}$ to the primary astrocytes cells was confirmed (**Figure 4**a). There seemed to be a trend of increased viability due to the presence of the HVs that might be attributed to higher metabolic activity since the assay monitored the cellular dehydrogenase activity. In astrocytes, the astrocyte-neuron lactate shuttle hypothesis suggests that the glial glucose metabolism is almost completely anaerobic, and that the generated lactate, which is released is transferred to neurons.[16] Thus, the higher metabolic activity may be explained by increased levels of lactate dehydrogenase A (LDHA) activity, which converts pyruvate into lactate. Furthermore, a switch in the astrocytic metabolic pathways toward the activation pyruvate dehydrogenase (PDH), that converts pyruvate into Acetyl-CoA, may also justify our observations. Further experiments are necessary to address these questions in more detail. Alternatively, we could modulate the extracellular microenvironment by culturing astrocytes together with neurons and microglia or change the levels of glucose in order to change the levels of pyruvate, to evaluate the impact of HVs on the cell viability in these experimental conditions. These concepts are considered in our ongoing efforts.

Second, the amount of HVs positive cells was determined by flow cytometry using $^{mix1}HV_0$, $^{mix1}HV_{CL-1}$, and $^{mix1}HV_{CL-2}$ (Figure 4bi). The association of the HVs with the primary astrocytes increased within 24 h. Additionally, two astrocyte populations were found. A first population showed positive cells with a high association with HVs, while the second population had limited to no association with the HVs, as previously shown for the C8-D1A astrocyte cell line. Specifically, only ≈25% of the cell population associated with the HVs without statistically significant differences depending on the used type of HVs for all tested time points (Figure S5, Supporting Information). With the aim to increase the number of cells in the population that associated with the HVs, we replaced the media containing the first dose of HVs with media that had a second dose of HVs and let to incubate for additional 24 h before analysis by flow cytometry. The double dose resulted in ≈50% and ≈30% of the cell population associating with $P1^{OG}$ and $^{Rho}PE$, respectively. This finding was surprising since the two building blocks were assembled into HVs, suggesting accumulation of $P1^{OG}$ while $^{Rho}PE$ was exocytosed within 24 h.

In addition, we followed the CMF of the positive cells over 24 h (Figure 4bii). As expected, the CMF originating from $P1^{OG}$ and $^{Rho}PE$ increased over time without any statistically significant differences depending on the type of HVs. Interestingly, not only the number of cells in the population that associated with $P1^{OG}$ but also their CMF originating from $P1^{OG}$ continuously increased over 24 h. In contrast, the CMF coming from $^{Rho}PE$ was close to saturation after 3 h incubation. Although second dose of HVs and an additional 24 h incubation showed a trend of increased CMF originating from both $P1^{OG}$ and $^{Rho}PE$, the increase was not statistically significantly higher compared to 24 h incubation with the first HVs dose. However, the difference in CMF originating from $P1^{OG}$ after the second dose of HVs was statistically significantly higher compared to 6 h incubation with the first dose of HVs in all cases, suggesting polymer accumulation over time. Complementarily, we stained the lysosomes of primary astrocytes double-dosed with $^{mix1}HV_0$, $^{mix1}HV_{CL-1}$, and $^{mix1}HV_{CL-2}$ for visualization by CLSM (Figure 4c). As expected from the flow cytometry data, only few primary cells exhibited fluorescent signals coming from the building blocks of the HVs. Although there were indications that the signal originating from $P1^{OG}$ was not always overlapping with a stained lysosome, a more detailed analysis (e.g., Pearson correlation coefficient determinations) was impossible due to the low number of cells with internalized HVs.

As previously mentioned, astrocytes play key function in the brain functioning, such as the modulation of synaptic formation and synaptic transmission, BBB formation and control of blood flow, metabolic support of other brain cells, which is pointed to be related with the astrocyte heterogeneity in the brain. Batiuk and collaborators have identified five transcriptomically distinct astrocyte subtypes in adult mouse cortex and hippocampus.[17] Since the primary astrocyte culture used here was prepared from the cortex and the hippocampus, the substantial variability in HV uptake between cells that we observed is probably related to the astrocyte heterogeneity in the brain.

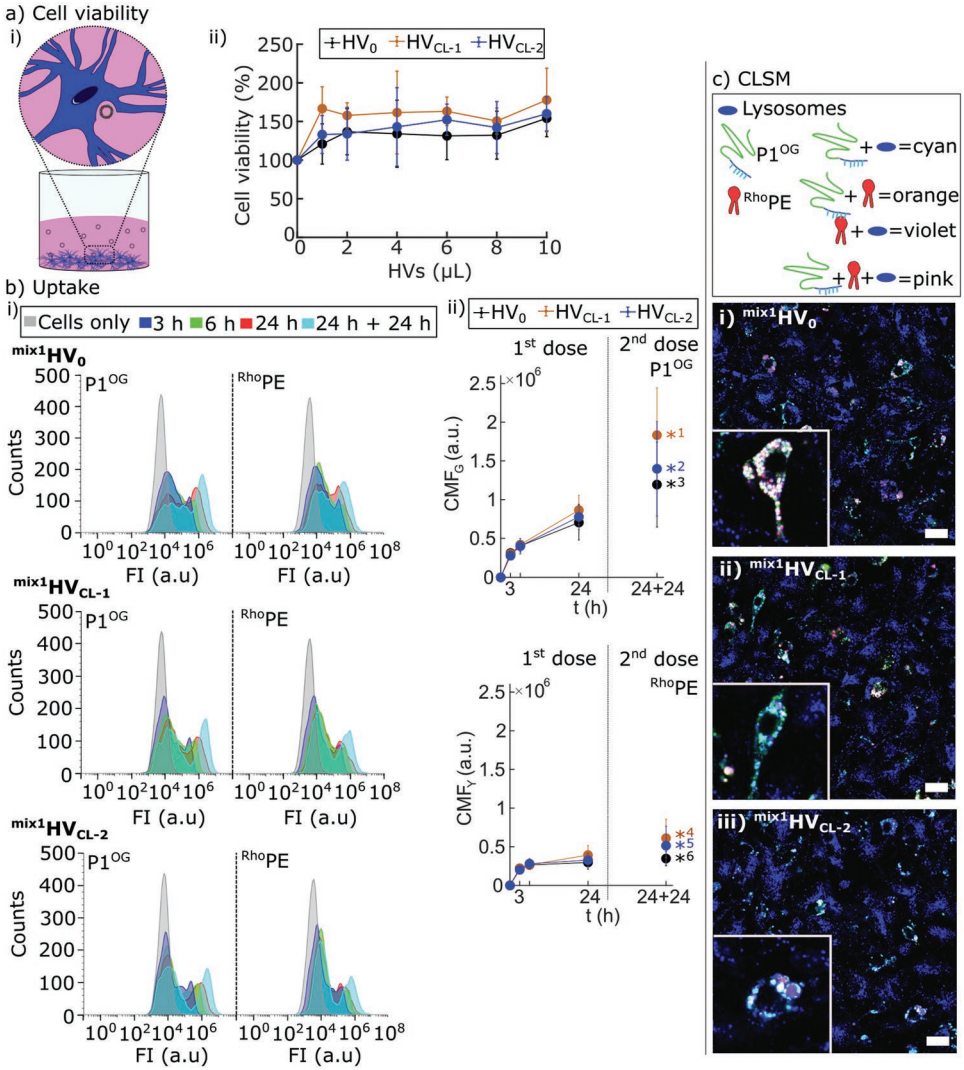


**Figure 4.** Primary astrocytes–HV interaction in 2D culture: a) i) Cartoon showing interaction of astrocytes with HVs. ii) Short-term viability of primary astrocytes exposed to $HV_0$, $HV_{CL-1}$, and $HV_{CL-2}$ for 24 h. The data are expressed as mean ± SD ($n = 3$, independent cultures performed in triplicates). b) i) Representative histograms obtained by flow cytometry of cells incubated with $^{mix1}HV_0$, $^{mix1}HV_{CL-1}$, and $^{mix1}HV_{CL-2}$ for 24 h ($n = 3$, independent cultures performed in triplicates). ii) Cell mean fluorescence (CMF) of primary astrocytes after exposure to a first dose of $^{mix1}HV_0$, $^{mix1}HV_{CL-1}$, and $^{mix1}HV_{CL-2}$ for 3, 6, and 24 h followed by 24 h incubation with a second dose of $^{mix1}HV_0$, $^{mix1}HV_{CL-1}$, and $^{mix1}HV_{CL-2}$ ($P1^{OG}$: green channel; $^{Rho}PE$: yellow channel). The data are expressed as mean ± SD, $*p < 0.05$. Comparing in the green channel: 1) $^{mix1}HV_{CL-1}$ at 48 h compared to 0, 3, 6, and 24 h within the same sample, 2) $^{mix1}HV_{CL-2}$ at 48 h compared to 0, 3, and 6 h within the sample, 3) $^{mix1}HV_0$ at 48 h compared to 0, 3, and 6 h within the same sample. Comparing in the yellow channel: 4) $^{mix1}HV_{CL-1}$ at 48 h compared to 0, 3, and 6 h within the same sample, 5) $^{mix1}HV_{CL-2}$ at 48 h compared to 0 h within the same sample, 6) $^{mix1}HV_0$ at 48 h compared to 0 h within the same sample. c) Representative CLSM images of cells incubated with two doses of $^{mix1}HV_0$, $^{mix1}HV_{CL-1}$, and $^{mix1}HV_{CL-2}$ (total incubation time 48 h, second dose 24 h after the first dose) (blue: LysoTracker Deep Red stained lysosomes; green: $P1^{OG}$; red: $^{Rho}PE$). Scale bars are 20 µm.

### 2.3. Astrocytes in Floating Paper Chips

Although tissue-culture polystyrene is widely used, it does not offer the 3D soft environment cells experience in a living organism. Paper-based cell cultures are an emerging alternative where the moist cellulose fibers offer a more realistic surroundings for the cells. Paper chips have previously been used for cardiac,[18] bone,[19] and liver tissue.[20] Primary astrocytes, which were cultured in parafilm-supported cellulose filter paper, had a positive effect on the cell viability of neurons in their proximity.[21] Inspired by the concept from Agarwal et al.,[20b] we demonstrated that floating, structured paper chips could be used to co-culture Caco-2 cells and HT29-MTX-E12 cells toward an intestinal cell models,[15] or as scaffold at the air-liquid interface for keratinocytes.[22]

Here, we used the same type of paper chip design for the culture of the astrocytes. However, in addition to the previously used 520 µm thick paper chips (referred to as paper chip 1), we also employed a thinner paper chip with only 180 µm thickness (referred to as paper chip 2). The desired shape was printed in an inkjet printer using commercial ink that melted during autoclaving resulting in hydrophobic barriers. The entire

cross-section of the paper in paper chip 2 was infiltrated with ink (Figure S6, Supporting Information), while we had previously observed that the middle part of the cross-section in paper chip 1 remained ink free.

### 2.3.1. C8-D1A Astrocytes Cell Line

First, we used different seeding densities in untreated and poly(L-lysine) (PLL) coated paper chips 1 with a diameter of 3 mm. The cells were let to grow in the paper chips for 14 days before live/dead staining and imaging by CLSM (Figure S7, Supporting Information). Only a seeding density of 75 000 cells per paper chip 1 resulted in a highly populated scaffold after 14 days with no obvious differences between PLL coated and pristine paper chips 1. There were still unoccupied areas between the cell clusters for lower seeding densities. It should be noted that when using paper chips 1 with a diameter of 6.7 mm, the C8-D1A astrocytes proliferation was limited after 9 days even for a 75 000 cell seeding density (Figure S8, Supporting Information). Therefore, only paper chips with a 3 mm diameter were used for all further experiments.

With the aim to follow the C8-D1A astrocytes proliferation in more detail, 75 000 and 150 000 cell seeding densities were used in untreated paper chips 1 and paper chips 2, and the cells in the chips were live/dead stained and imaged by CLSM after 3, 9 and 14 days in culture (**Figure 5**a). Importantly, the C8-D1A astrocytes proliferated in all cases. However, the cells cultured in paper chip 1 seemed less spread in the 3D environment of the paper fibers even after 14 days. This observation might be due to the thickness of the paper that limited the detection of the emitted fluorescence. In contrast, the thinner paper chip 2 likely facilitated better fluorescence emission and the 3D occupation by the C8-D1A astrocytes was visible especially after 3 and 9 days when the cells were not as dense as after 14 days.

In addition, we monitored the cell proliferation quantitatively using the MTT assay (Figure 5b). All conditions showed proliferation over 14 days, and the 150 000 cell seeding density showed the expected higher number of cells present compared to a 75 000 cell seeding density. No significant differences were observed between paper chips 1 and 2, that is, the thickness of the paper did not have an impact on the proliferation of the astrocytes.

Further, we determined if C8-D1A astrocytes cultured in paper-based chips preserved their cell type specific calcium signalling function. Therefore, 75 000 cells were seeded in paper chip 1 and cultured for 14 days before staining with the Fluo-4 NW Calcium Assay Kit. The calcium release by the C8-D1A astrocytes was stimulated with 100 µM ATP immediately before time-lapse images were recorded using the CLSM for 5 min (2 frames $min^{-1}$). The calcium release spiked after ≈90 s and was followed by the decay to the baseline signal (**Figure 6**a, Movie S1, Supporting Information). The fluorescent intensity of 4 representative C8-D1A astrocytes was followed over time using the Fiji plugin Time Series Analyzer V3 to get a semi-quantitative determination of the calcium signalling. The fluorescence intensity increased at different time points for different cells as it was expected that not all cells are simultaneously responding to the added ATP. A number of C8-D1A astrocytes was activated twice by the ATP within the recorded

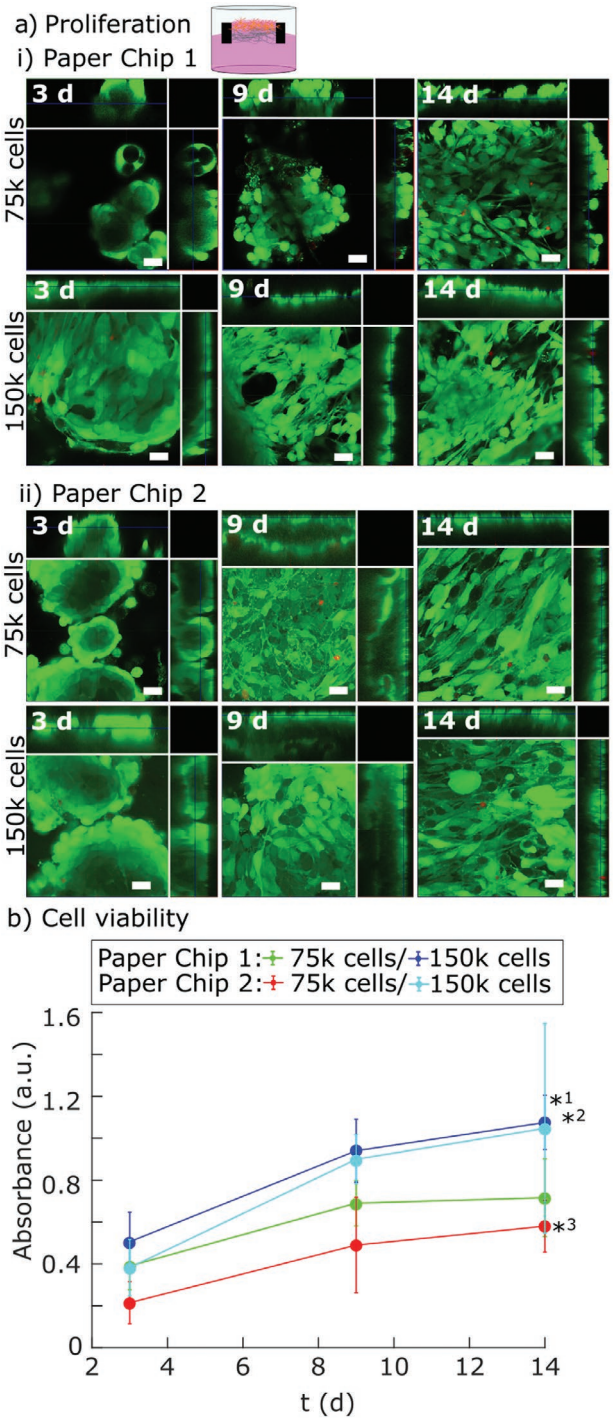


**Figure 5.** C8-D1A astrocytes in paper chips – proliferation: a) Representative CLSM images of C8-D1A astrocytes cultured in uncoated paper chip 1 i) and paper chip ii) for 3, 9, or 14 days using a seeding density of either 75 000 cells (top row) or 150 000 cells (bottom row). The side-views of 3D images are shown on top and right of the CLSM images (green: calcein-AM, red: ethidium homodimer-1; $n = 2$). Scale bars are 20 µm. b) Metabolic activity of cells cultured in uncoated paper chips 1 or 2 was assessed using an MTT assay (seeding density of either 75 000 cells or 150 000 cells). The data are expressed as mean ± SD ($n = 3$) (*$p < 0.05$: 1) 150k cells in paper chip 1 compared to 75 000 cells in paper chip 1 or 2; 2) 150 000 cells in paper chip 1 compared to itself at 3 and 14 days; 3) 75 000 cells in paper chip 2 compared to itself at 3 and 14 days).

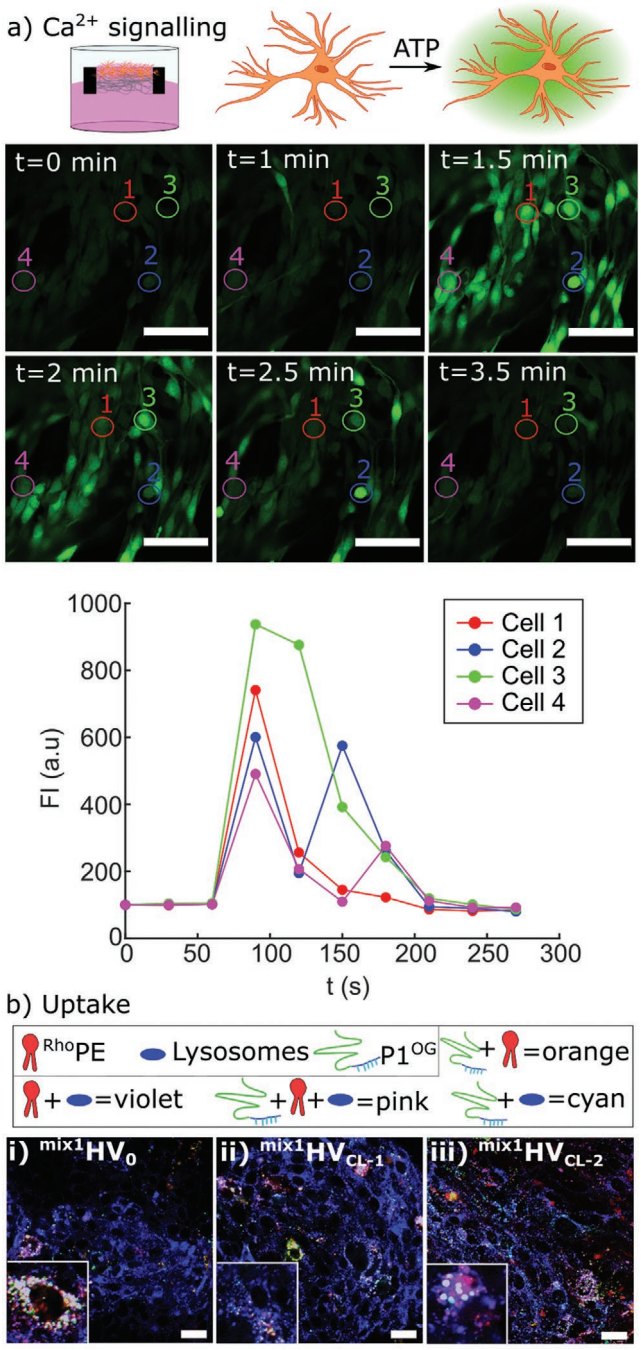


**Figure 6.** C8-D1A astrocytes in paper chips: a) i) Representative CLSM images of C8-D1A astrocytes cultured in paper chip 1 for 14 days incubated with fluo-4 that showed the cellular calcium signalling over time ($n = 2$). Scale bars are 50 µm. ii) Analysis of the fluorescent signal originating from the selected cells over time. b) Representative CLSM images of C8-D1A astrocytes cultured in paper chip 1 for 14 days incubated with $^{mix1}HV_0$, $^{mix1}HV_{CL-1}$, and $^{mix1}HV_{CL-2}$ for 24 h (blue: LysoTracker Deep Red stained lysosomes; green: $P1^{OG}$; red: $^{Rho}PE$; $n = 2$). Scale bars are 20 µm.

time frame, an aspect previously observed for astrocytes.[23] The calcium signalling of C8-D1A astrocytes cultured in polystyrene tissue culture 96-well plates stimulated by histamine and ATP was confirmed by measuring the fluorescence intensity of the Fluo-4 with a microplate reader and an inverted wide-field microscope (Figure S9 and Movie S2, Supporting Information).

Finally, the uptake of the HVs by C8-D1A astrocytes cultured in paper-based chips was explored. To this end, 75 000 cells were seeded in paper chip 1 and let to proliferate for 14 days before 50 µL HV stock solution was added and incubated with the cells for 24 h. The lysosomes of the C8-D1A astrocytes were stained with LysoTracker Deep Red before visualization by CLSM with the aim to identify the location of the HVs (i.e., the fluorescently labeled building blocks) following endocytosis (Figure 6b). All three types of HVs were internalized, but only ≈10% of the C8-D1A astrocytes had fluorescent signal originating from either $P1^{OG}$ or $^{Rho}PE$. The HV internalization by C8-D1A cells that were cultured in standard tissue-culture polystyrene plates was seemingly higher. However, it was more challenging to image the cells in the paper chips, and the estimation of the uptake efficacy had limited accuracy.

### *2.3.2. Primary Astrocytes*

Complementary, we evaluated the adhesion and survival of primary astrocytes to the paper chips 1 and 2 that were either uncoated or poly(D-lysine) (PDL) coated seeding 75 000 or 150 000 cells per paper chip and letting the primary astrocytes mature for 14 days before live/dead staining and visualization by CLSM (**Figure 7**a). The images revealed that most cells were viable, and the cells started to form larger connected clusters with processes that indicated matured astrocytes. However, 75 000 cell densities were too low to ensure coverage of the entire white area in both types of paper chips. The coating with poly-D-lysine did not show any benefit, which was in contrast to findings previously seen for poly-D-lysine coated tissue culture polystyrene substrates. There was no difference in cell density observable in paper chip 1 depending on the seeding density. We attributed this observation to the fact that the seeded primary astrocytes, which could only mature but not proliferate, were too few to cover the entire fiber volume in the thick the paper chip 1. This aspect was supported by a higher number of detectable primary astrocytes in paper chip 2 when using 150 000 cells for seeding.

In addition, the presence of the GFAP, which is an intermediate filament protein expressed primary in mature astrocytes, was confirmed. To this end, primary astrocytes (150 000 seeding density) matured for 14 days in paper chip 2 were immunostained with anti-GFAP. The nuclear envelope was also marked using anti-lamin B1 for better visualization of the cells by CLSM (Figure 7b, left image). The primary astrocytes showed high expression of GFAP illustrating that they preserved their phenotype. The 3D nature of the cell culture became also very visible in the CLSM images since the stained processes were present throughout multiple imaging planes. It should be noted that the primary astrocytes also adhered to black part of the paper chip with preserved GFAP expression capability (Figure 7b, right image). In this case, the cells grew more 2D-like since the molten ink resembled the polystyrene substrates.

Further, the primary astrocytes were cultured in paper-based chip 2 preserved their cell type specific calcium signalling function using the protocol outlined above (Figure 7c, Movie S3, Supporting Information). The primary astrocytes showed

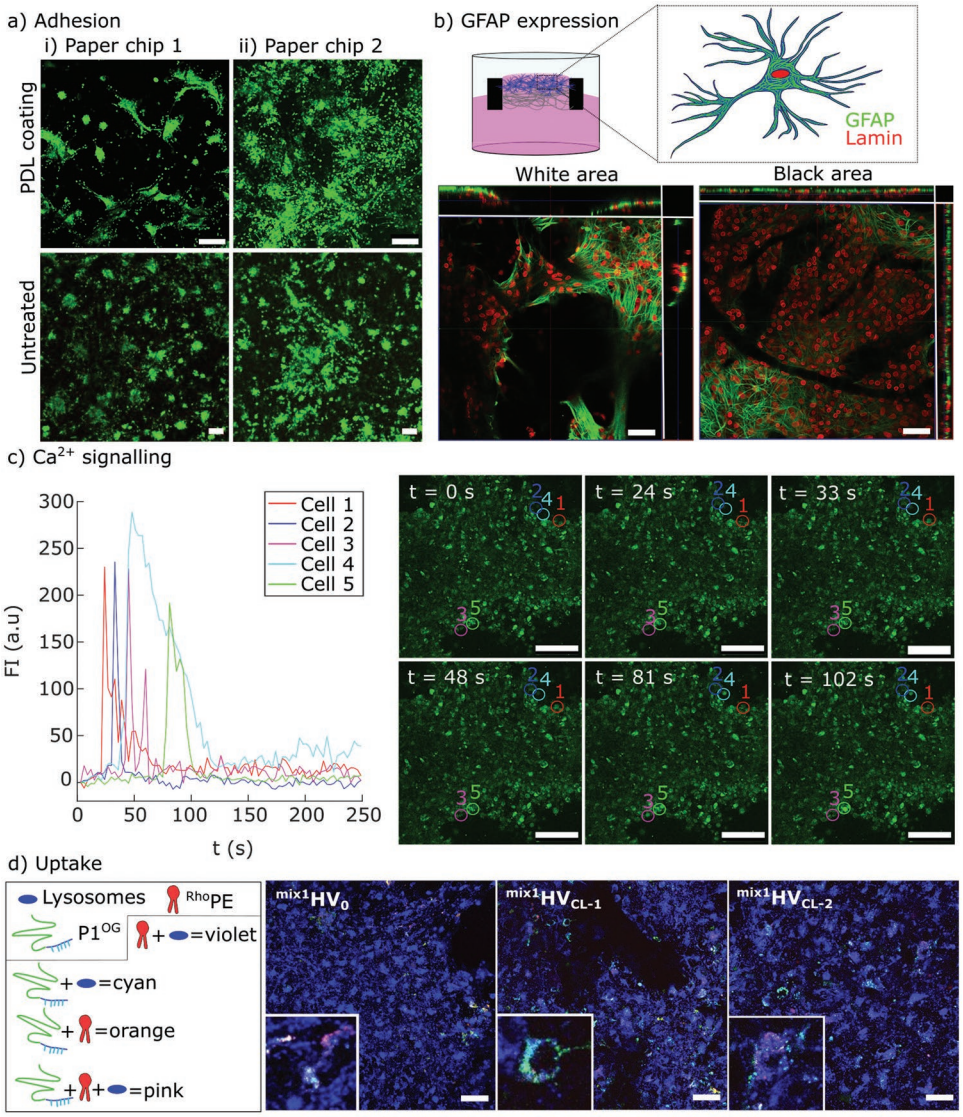


**Figure 7.** Primary astrocytes in paper chips: a) Representative CLSM images of primary astrocytes matured i) in uncoated and PDL coated paper chip 1 and paper chip 2 ii) for 14 days using a seeding density 150 000 cells. (green: calcein-AM, red: ethidium homodimer-1). Scale bars are 200 µm. b) Representative CLSM images of primary astrocytes matured for 14 days i) in the uncoated part or ii) the printed area of paper chip 2 with stained GFAP as an astrocyte marker (green) and lamin as a nuclei marker (red). The side-views of 3D images are shown on top and right of the CLSM images. Scale bars are 50 µm. c) i) Representative CLSM images of primary astrocytes cultured in paper chip 2 for 14 days incubated with Fluo-4 which showed the cellular calcium signalling over time. Scale bars are 100 µm. ii) Analysis of the fluorescent signal originating from the selected cells over time. d) Representative CLSM images of primary astrocytes cultured in paper chip 2 for 14 days double dosed with $^{mix1}HV_0$, $^{mix1}HV_{CL-1}$, and $^{mix1}HV_{CL-2}$ (blue: LysoTracker deep Red stained lysosomes; green: $P1^{OG}$; red: $^{Rho}PE$). Scale bars are 50 µm.

a fast calcium transient state due to the activation of specific Gq-protein coupled ATP receptors expressed in astrocytes, in accordance with previous studies.[24]

Finally, we exposed primary astrocytes cultured in paper chip 2 for 14 days to a double dose of $^{mix1}HV_0$, $^{mix1}HV_{CL-1}$, and $^{mix1}HV_{CL-2}$ before staining the lysosomes and visualization by CLSM (Figure 7d). The primary astrocytes internalized the different types of HVs at a very low level. This latter aspect made it difficult to draw detailed conclusions. However, there were indications that the building blocks of $^{mix1}HV_0$ were co-localized with the lysosomes. In contrast, primary astrocytes exposed to $^{mix1}HV_{CL-1}$, and $^{mix1}HV_{CL-2}$ had localized fluorescent signal originating from $P1^{OG}$ that did not seem to be co-localized with either the signal from $^{Rho}PE$ or the lysosomes, suggesting that cytosolic placement of $P1^{OG}$. This aspect was distinctively different to primary astrocytes cultured in well plates, indicating an impact on of the 3D environment on the cells' interaction with and processing of the vesicles.

## 3. Conclusion

We explored the culturing of C8-D1A astrocytes and primary astrocytes in paper chips and their interaction with HVs.

We demonstrated that the membrane of the HVs could be crosslinked, which resulted in HVs with higher stability and lower permeability. Both, the C8-D1A astrocytes and primary astrocytes proliferated and matured, respectively, in the paper chips with preserved calcium signalling ability. The HVs could be internalized by both types of astrocytes and in 2D and 3D cell culture, but to a rather low extent when primary astrocytes were used.

This effort is the stepping stone for equipping astrocytes with HV-based artificial organelles to endow them with either boosted or non-native function that could proof beneficial for their communication with neurons.

## 4. Experimental Section

*Materials*: 4-(2-hydroxyethyl)piperazine-1-ethane-sulfonic acid (HEPES, ×99.5%), sepharose 2B, Triton X-100 (TX), 6-dodecanoyl-*N*,*N*-dimethyl-2-naphthylamine (Laurdan), cell counting kit-8 (CCK-8), phosphate-buffered saline (PBS), 0.25% trypsin-ethylenediaminetetraacetic acid (trypsin-EDTA), poly(L-lysine) hydrobromide (PLL, Mw = 30–70 kDa), Whatman CF12 filter paper sheets (WHA10535097)), Dulbecco's Modified Eagle's Medium-high glucose, adenosine 5′-triphosphate (ATP) disodium salt hydrate, histamine dihydrochloride, bovine serum albumin (BSA), poly(D-lysine) (PDL, Mw = 30–70 kDa), paraformaldehyde (PFA), anti-GFAP antibody (clone GA5), Tetrahydrofuran (THF), sodium chloride (NaCl), hydrochloric acid (HCl), sodium hydroxide (NaOH), *N*-3-(3-dimethylaminopropyl)carbodiimide hydrochloride (EDC), and *N*-hydroxysulfosuccinimide (NHS) were purchased from Sigma Aldrich. Cytotoxicity assay kit (MTT) and quantitative filter paper 600 (516-0309) were purchased from VWR. LIVE/DEAD Viability/Cytotoxicity Kit for mammalian cells, Fluo-4 NW Calcium Assay Kit, Alexa Fluor 488 donkey anti-mouse IgG (H+L), Alexa Fluor 568 donkey anti-rabbit IgG (H+L) and LysoTracker Deep Red were obtained from Thermo Fisher Scientific. 1,2-Dioleoyl-*sn*-glycero-3-phosphocholine (DOPC), 1,2-dioleoyl-*sn*-glycero-3-phosphoethanolamine (DOPE), 1,2-dipalmitoyl-*sn*-glycero-3-phosphoethanolamine-*N*-(7-nitro-2-1,3-benzoxadiazol-4-yl) ($^{NBD}$PE) and 1,2-dimyristoyl-*sn*-glycero-3-phosphoethanolamine-*N*-(lissamine rhodamine B sulfonyl) ($^{Rho}$PE) were purchased from Avanti Polar Lipids. Fetal bovine serum (FBS) was purchased from Invitrogen. Anti-Lamin B1 antibody was purchased from Abcam.

HEPES buffer consisted of 10 mM HEPES and 150 mM NaCl at pH 7.4. Ultrapure water (18.2 MΩ cm resistance) was provided by an ELGA Purelab Ultra system (ELGA LabWater, Lane End).

Poly(cholesteryl methacrylate)-*block*-poly(2-carboxyethyl acrylate) (P1) and Oregon green-labeled polymer ($P1^{OG}$) were synthesized as previously described.[15]

Rhodamine-labeled P1 ($P1^{Rho}$) was made by dissolving P1, EDC (20 mg, 0.12 mmol), and NHS (20 mg, 0.16 mmol) in THF and dropwise addition of Lissamine Rhodamine B Ethylenediamine (170 µL, 10 mg mL$^{-1}$ in DMSO). The solution was stirred for 12 h and purified by dialyzing against water before freeze-drying.

$^1$H NMR (400 MHz, THF-d8) δ (ppm): 0: 0.6-2.6 (polymer backbone), 4.3 (br,−CO−O−$CH_2$−$CH_2$−COOH (CEA)), 4.48 (br, −CO−O−CH−($CH_2$−)$_2$ and 5.4 (br, −C*H*=C−), 5.38 (s), 6.9(s), 7.12(br), 7.91(s) and 10.785(s) (aromatic, Rho).

*HV Assembly and Characterization*: HV assembly was performed with the film rehydration method. 0.4 mg of P1 (5 mg mL$^{-1}$ in THF) was mixed with 1.1 mg DOPE (25 mg mL$^{-1}$ in chloroform) in a 25 mL round-bottom flask and dried using a rotary evaporator (Heidolph G5) for 15 min, then, the flask was attached to the vacuum line overnight for further drying. Then, 1 mL HEPES buffer (pH = 9.1) was added followed by alternately sonicating for 10–20 s and vortexing for 10–15 min. The solution was extruded through 400 nm membrane (21×) and then 100 nm membrane (21×) at room temperature using a Mini-Extruder (Avanti Polar Lipids). The solution was split into three parts of equal volume. Two samples were crosslinked using EDC/NHS chemistry, and the third sample was left non-crosslinked referred to as $HV_0$. $HV_{CL\text{-}1}$, which had a low crosslinking density, was obtained by adding 0.201 mg NHS and 0.180 mg EDC dissolved in HEPES buffer. $HV_{CL\text{-}2}$ had a higher crosslinking density and was obtained by adding 0.412 mg NHS and 0.360 mg EDC. The samples were let to crosslink overnight (pH 8). Finally, the samples were purified via size exclusion chromatography (SEC, Sepharose 2B) to separate the HVs from micelles and other small components. Fluorescently labeled HVs were assembled by adding 0.4 mg $P1^{OG}$ or $P1^{Rho}$ (5mg mL$^{-1}$ in THF) and 1.063 mg DOPE and 0.037 mg $^{Rho}$PE (1 mg mL$^{-1}$ in chloroform) or 1.063 mg DOPE (25 mg mL$^{-1}$ in chloroform) and 0.037 mg $^{NBD}$PE (1 mg mL$^{-1}$ in chloroform), respectively, and referred to as $^{mix1}$HV and $^{mix2}$HV where mix1 corresponded to $P1^{OG}$ and $^{Rho}$PE and mix2 corresponded to $P1^{Rho}$ and $^{NBD}$PE. The HVs were stored in the fridge (4 °C) before usage. A detailed overview of the used building blocks for the HVs assembly can be found in Table S1, Supporting Information.

The hydrodynamic diameter ($D_h$) and the polydispersity index (PDI) of the HVs were determined by DLS (Malvern Zeta sizer Nano-590 at $\lambda$ = 632 nm at 25 °C). The stability of the HVs was tested in HEPES buffer or in HEPES buffer containing 0.02% TX final concentration.

The HVs were visualized using negative staining TEM. The grids were prepared by first adding 3 µL HV stock solution onto a glow-discharged 300 mesh copper formvar/carbon grid, which was left to adsorb for 30 s before blotting the excess sample. The grids were then stained once with 3 µL of 2% uranyl acetate for 2 s. TEM images were taken using a Tecnai G2 Spirit instrument (TWIN/BioTWIN, FEI Co.). At least 30 min were used on searching each grid of samples treated with TX, to ensure whether vesicular assemblies were present. The size distribution of the vesicles was calculated from the TEM images by measuring at least 100 vesicles using Fiji software. A LogNormal curve was used to fit the histograms and the sizes were given as mean */for 95.4% of the population.

Cryo-EM grids were prepared by adding 3 µL HVs solution onto a 1.2/1.3 um 300 mesh C-flat grid. The grids were plunge-frozen in liquid ethane using a Mark IV vitrobot (Thermo Fisher) with a blotting time of 4.5 s. The vitrified cryo-EM grids were imaged Titan Krios with an X-FEG operated at 300 kV. Movies were acquired using a Gatan K2 camera with a Bioquantum energy filter operated at a slit width of 20 eV. A nominal magnification of 165 000× and a pixel size of 0.835 Å were used. Exposures of 7.6 s fractioned into 38 frames were collected through EPU software (Thermo Fisher) at a dose rate of 60 e$^-$ per Å$^2$.

The emission spectra of the HVs were obtained by adding 100 µL of the HVs to a black 96-well plate and recording from $\lambda_{em}$ = 503–650 nm using an excitation wavelength of $\lambda_{ex}$ = 488 nm. TX was added to the HVs to a final concentration of 0.1% or 0.02%TX, then, the emission spectra were re-recorded immediately and after 3 h incubation at room temperature. The emission spectra of the $P1^{Rho}$ present in $^{mix2}HV_0$, $^{mix2}HV_{CL\text{-}1}$, and $^{mix2}HV_{CL\text{-}2}$ were recorded by adding 100 µL of the HVs to a black 96-well plate and recording from $\lambda_{em}$ = 565–700 nm using an excitation wavelength of $\lambda_{ex}$ = 550 nm. The FRET data were normalized to the fluorescence intensity at $\lambda_{em}$ = 565 in each measurement to correct for different fluorescent intensities between the different batches.

The pH sensitivity of the HVs was assessed using DLS. $D_h$, PDI, and correlograms of $HV_0$, $HV_{CL\text{-}1}$, or $HV_{CL\text{-}2}$ were obtained before and after decreasing the pH to 4 by adding 5–8 µL HCl (1 M) and 5–8 µL NaOH to increase the pH back to 7.

The membrane fluidity was assessed using the fluorescence probe Laurdan. 25 µL of unlabeled HVs, 75 µL of HEPES, and 2.5 µL stock solution of Laurdan (stock solution 100 µM in DMSO) was added to a black 96-well plate (100 µL final volume, 2.5 µM final concentration Laurdan). The plate was shaken for 45 min (300 rpm) and the emission spectra were recorded using an excitation wavelength $\lambda_{ex}$ = 340 nm ($\lambda_{em}$ = 390–590 nm). The general polarization value (GP) was calculated using

$$GP = \frac{I_{490} - I_{440}}{I_{490} + I_{440}} \quad (1)$$

where $I_{440}$ and $I_{490}$ are the emission intensities at $\lambda_{em}$ = 440 and $\lambda_{em}$ = 490 nm, respectively.

The permeability of the HVs was assessed using dithionite. After the stabilization of the fluorescence intensity (≈300 s), 10 µL dithionite (20 mM in Tris pH 10) was added having a final concentration of 2 mM, and the decrease of fluorescence intensity was measured over ≈600 s. The data was normalized dividing by the maximum value and the linear decay of each of the repeats was fitted to a linear regression to calculate the slope. The statistical significance was determined using one-way ANOVA followed by a Tukey's multiple comparison test ($^*p \leq 0.05$).

*GUV Assembly*: GUVs were assembled by electroformation. 10 µL of DOPC (25 mg mL$^{-1}$ in chloroform) and 20 µL of chloroform were mixed in a vial and the mixture was evenly spread to a thin layer of indium tin oxide (ITO)-coated glass coverslips (VesiclePrepChamber, Nanion Technologies GmbH). The coverslip was let to dry overnight in a vacuum chamber. An 18 mm × 1 mm O-ring was placed on this coverslip and another ITO-coated coverslip was placed on top. The space between the coverslips was filled with 280 µL of buffer solution (300 mM sucrose and 1 mM HEPES) to rehydrate the lipid film. An AC electric field (5 V, 10 Hz) was applied for 2 h at 26 °C to generate the GUVs. The GUVs were stored at 4 °C.

In order to visualize the interaction of $^{mix2}HV_0$, $^{mix2}HV_{CL\text{-}1}$, or $^{mix2}HV_{CL\text{-}2}$ with unlabeled DOPC GUVs, 2–5 µL of GUV solution was added on top of 25 µL of HEPES buffer on a glass coverslip. Then, 20–25 µL of HV ($^{mix2}HV_0$, $^{mix2}HV_{CL\text{-}1}$, or $^{mix2}HV_{CL\text{-}2}$) solution was added. The interaction was visualized using a Zeiss LSM700 confocal laser scanning microscope (CLSM) (Carl Zeiss, Germany) where at least 4 images per sample were taken. Then, the pH was lowered to 4–5 by addition of 1–2 µL of HCl (0.5 M), and at least 4 areas were recorded. Finally, the pH was increased back to 7 by addition of 1–2 µL of NaOH (0.5 M), and at least 4 areas were recorded. Two independent batches of vesicles were imaged using a 63× objective (6% laser gain, 70 µm pinhole) and two imaging channels: green emission ($^{NBD}$PE) $\lambda_{ex}$ = 488 nm and $\lambda_{em}$ = 518 nm; and red emission ($P1^{Rho}$): $\varpi_{ex}$ = 555 nm and $\lambda_{em}$ = 573 nm.

*Paper Chip Preparation*: The paper chips were inspired by the previously reported approach described by Agarwal et al.[20b] and were designed and fabricated as outlined in the previous effort.[15] The resulting circular paper chips were a non-printed ring with an inner diameter of 0.67 cm and an inkjet printed ring with an inner diameter of 0.30 cm. The rings were printed double-sided on A4 Whatman filter paper (520 µm, paper chip 1) and VWR qualitative filter paper 600 (516-0309) (180 µm, paper chip 2) using a LaserJet printer (Xerox WorkCentre 7845). The paper sheets were autoclaved to melt the ink particles to make hydrophobic barriers on the paper chips that allowed the paper chips to float. The morphological characteristics of the paper chips were visualized using scanning electron microscopy (SEM). Images were taken in a Nova nanoSEM 600, operating at 5 kV and a working distance of 6 mm, with an ETD detector. The samples were mounted on carbon-taped microscopy stubs and coated with a thin layer of platinum (6 nm).

The paper chips were used either untreated or coated with PLL. The PLL or PDA coatings were performed by adding 30 µL polypeptide solution (1 mg mL$^{-1}$ in ultrapure water) on top of the paper chips floating on cell media and incubation for 15 min at 37 °C and 5% $CO_2$.

*Cell Work—C8-D1A Astrocyte Cell Line*: The C8-D1A astrocyte cell line was obtained from European Collection of Authenticated Cell Cultures. The cells were cultured at 37 °C and 5% $CO_2$ in a 75 cm$^2$ culture flask in Dulbecco's Modified Eagle's Medium with 4500 mg L$^{-1}$ glucose, sodium pyruvate, and sodium bicarbonate. The medium was supplemented with 10% FBS and 1% streptomycin/penicillin. The media was changed every second day, and the cells were split at 90% confluency.

*Cell Viability—HVs*: The C8-D1A astrocyte was seeded in a 96-well plate (75 000 cells per wells in 100 µL media) and incubated at 37 °C and 5% $CO_2$ to adhere overnight. Different concentrations of HVs in HEPES buffer were added to the cells with a max of 10 v/v% and left to incubate for 24 h at 37 °C and 5% $CO_2$. Then, the media in each well was replaced with 100 µL new media mixed with 10 µL CCK-8 assay solution and incubated for 1 h at 37 °C and 5% $CO_2$. The absorbance was measured at $\lambda_{abs}$ = 450 nm in a multi-plate reader. The data were normalized to the fluorescence of the cells only without the HVs. Three independent repeats were performed.

*HV Uptake*: The C8-D1A astrocytes were seeded in a 96-well plate (75 000 cells per well in 100 µL media) and allowed to adhere overnight at 37 °C and 5% $CO_2$. 10 µL of the fluorescently labeled HVs ($^{mix1}HV_0$, $^{mix1}HV_{CL\text{-}1}$ and, $^{mix1}HV_{CL\text{-}2}$) were added to the wells and let to incubate with the cells for 3, 6, and 24 h before harvesting the cells by washing them twice with PBS before using trypsin-EDTA for cell detachment (30 µL, 5 min, 37 °C and 5% $CO_2$) followed by addition of 125 µL media for neutralization. The fluorescence was measured by flow cytometry (Guava easyCyte Single Sample Flow Cytometer, Merck) using $\lambda_{ex}$ = 488 nm and $\lambda_{em}$ = 495–555 nm in the green channel (to detect $P1^{OG}$) and $\lambda_{em}$ = 557–609 nm in the yellow channel (to detect $^{Rho}$PE). At least 5000 cells were measured in triplicates for each sample and three independent repeats were performed. The fluorescence in each channel was analyzed by plotting the histogram for the green and yellow fluorescence followed by gating the cells into two populations. Population 1 was created from the samples containing cells only and population 2 was for the cells with a fluorescence signal higher than that. The percentage of cells that had an uptake and the CMF in the green and yellow channels for these cells were identified.

Additionally, the internalization of the HVs ($^{mix1}HV_0$, $^{mix1}HV_{CL\text{-}1}$, and, $^{mix1}HV_{CL\text{-}2}$) in the C8-D1 astrocytes was visualized by CLSM. To this end, 100 000 cells were seeded in a confocal dish (35 mm, VWR) and incubated for 3 days at 37 °C and 5% $CO_2$. The media was replaced with 1 mL media containing 50 µL HVs ($^{mix1}HV_0$, $^{mix1}HV_{CL\text{-}1}$, and, $^{mix1}HV_{CL\text{-}2}$) followed by 24 h incubation at 37 °C and 5% $CO_2$. The cells were washed twice with PBS and stained with 120 µL LysoTracker Deep Red diluted to 50 nM in pre-warmed media followed by 45 min incubation at 37 °C and 5% $CO_2$. The cells were washed twice with PBS and 170 µL PBS was added for storage. The cells were visualized by CLSM using a 40× objective. The lipids ($^{Rho}$PE) in the HVs were visualized using a $\lambda_{ex}$ = 572 nm and $\lambda_{em}$ = 590 nm, the $P1^{OG}$ in the HVs was visualized using a $\lambda_{ex}$ = 498 nm and $\lambda_{em}$ = 526 nm, and the lysosomes in the cells were visualized using a $\lambda_{ex}$ = 646 nm and $\lambda_{em}$ = 664 nm.

*Calcium Release*: The cells were seeded in a black 96-well plate with a cell density of 30 000, 50 000, and 75 000 cells well$^{-1}$ and incubated at 37 °C and 5% $CO_2$ overnight for adhesion. The calcium release was measured with the multi-plate reader using a Fluo-4 NW Calcium Assay Kit. Fluo-4 NW is a fluorescent calcium indicator that increases its fluorescence intensity upon binding to calcium. The cells were washed twice with PBS after which 100 µL of the Fluo-4 staining solution (prepared according to the manufacturer's instructions) was added followed by 45 min incubation at 37 °C and 5% $CO_2$. Before adding the stimuli for calcium release (ATP and histamine) the background fluorescence was measured for 2 min every 10 s at $\lambda_{em}$ = 516 nm using an excitation wavelength of $\lambda_{ex}$ = 494 nm. The calcium release was stimulated by adding 10 µL of 1 mM ATP, 100 µM ATP, or 1 mM histamine (final concentration of 100, 10, and 100 µM, respectively) very quickly after which the fluorescence was measured for 6 min every 10 s at the same parameters as described earlier. The background fluorescence was subtracted and the signal was normalized to the highest signal. Three independent repeats were performed.

The calcium release was further measured with an inverted wide-field epifluorescence microscope (Olympus IX81, Olympus CellSens dimensions software). For that purpose, 75 000 cells were seeded in a transparent 96-well plate. The cells were stained with the Fluo-4 NW Calcium Assay Kit as previously described. The cells were stimulated with 100 µM ATP, after which a time-lapse was recorded with 4× magnification (5 min, 2 frame min$^{-1}$). Three independent repeats were performed.

*Cell Proliferation—Paper Chips*: The sterile untreated or PLL-coated paper chip 1 or paper chip 2 were let to float on 1 mL media in a 24-well plate. Different amounts of cells (30 000–125 000 cells) were added to the non-printed central part of each paper chip and left to incubate for 2–14 days at 37 °C and 5% $CO_2$. The culture media was changed every second day. Then, the paper chips were flipped and washed twice

with PBS. 1 mL of staining solution containing ethidium homodimer-1 ($4 \times 10^{-6}$ M final concentration) and calcein-AM ($2 \times 10^{-6}$ M final concentration) in PBS was added to each well and incubated for 45 min at 37 °C and 5% $CO_2$. The cells were visualized with CLSM using a 40× objective. The live cells stained with calcein-AM were visualized using a $\lambda_{ex} = 493$ nm and $\lambda_{em} = 514$ nm and the dead cells stained with ethidium homodimer-1 were visualized using $\lambda_{ex} = 528$ nm and $\lambda_{em} = 617$ nm.

Complementary, the cell viability was also assessed using an MTT viability assay on days 3, 9, and 14 when 75 000 or 150 000 cells were seeded in untreated paper chip 1 or paper chip 2. The paper chips were transferred to a new 24-well plate, flipped, and washed twice with PBS. 60 µL MTT labeling reagent was added to each well followed by 4 h incubation at 37 °C and 5% $CO_2$. Then, 600 µL formazan solubilization reagent was added to each well and incubated for an additional 18 h at 37 °C and 5% $CO_2$. 200 µL of the final solution was transferred to a 96-well plate and the absorbance at $\lambda_{abs} = 570$ nm was measured using the multimode plate reader. Three independent repeats were performed. The statistical significance was determined using one-way ANOVA followed by a Tukey's multiple comparison test ($^*p \leq 0.05$).

*Calcium Release—Paper Chips*: 75 000 cells were added to each paper chip 1 and incubated for 14 days at 37 °C and 5% $CO_2$. The calcium release was visualized by CLSM using a Fluo-4 NW Calcium Assay Kit. To this end, the paper chip 1 was washed twice with PBS, flipped, and transferred to a confocal dish that contained 1 mL of the dye solution (prepared according to manufacturers' instructions) and incubated for 1–2 h. The confocal dish was placed on the CLSM, and the calcium release was stimulated by adding 100 µL 1 mM ATP solution (prepared in assay buffer) on top of the paper. Time-lapse imaging (5 min, 2 frame $min^{-1}$) using a 40× oil objective was employed to visualize the calcium signalling ($\lambda_{ex} = 494$ nm and $\lambda_{em} = 516$ nm).

*Uptake of HVs—Paper Chips*: Paper chips 1 were seeded with 75 000 cells and left to incubate at 37 °C and 5% $CO_2$ for 14 days. Then, 50 µL HVs ($^{mix1}HV_0$, $^{mix1}HV_{CL\text{-}1}$, and $^{mix1}HV_{CL\text{-}2}$) were added to the non-printed central part on top of the paper chips and incubated for 24 h at 37 °C and 5% $CO_2$. The papers were flipped and washed twice with PBS before staining with 1 mL LysoTracker Deep Red staining solution (50 nM in pre-warmed media) followed by 45 min incubation at 37 °C and 5% $CO_2$. The cells in the paper chips were visualized by CLSM using a 40× oil objective. The lipids ($^{Rho}$PE) in the HVs were visualized using a $\lambda_{ex} = 572$ nm and $\lambda_{em} = 590$ nm, the $P1^{OG}$ in the HVs was visualized using a $\lambda_{ex} = 498$ nm and $\lambda_{em} = 526$ nm, and the lysosomes in the cells were visualized using a $\lambda_{ex} = 646$ nm and $\lambda_{em} = 664$ nm.

*Cell Work—Primary Astrocytes*: Cortical astrocytes were obtained from 0–2 days old Wistar pups. The cultures were prepared as reported previously by Vaz et al.[25] The pups were sacrificed by decapitation and the heads were sterilized by submersion into ethanol (70%) three times. Then, the heads were dissected in PBS solution. The cortex was mechanically dissociated by pipetting in Dulbecco's modified Eagle's medium (DMEM, 10 mL) supplemented with 10% (v/v) FBS and antibiotic/antimycotic solution (100 U $mL^{-1}$ penicillin, 0.25 µg $mL^{-1}$ amphotericin B and 100 µg $mL^{-1}$ streptomycin). The cell suspension was filtered through a 230 µm pore strainer followed by centrifugation (10 min at 200 rpm). Then, the supernatant was discarded, and the cells were re-suspended in 10 mL DMEM media. The latter was repeated using a 70 µm pore cell strainer and resuspension in 10 mL DMEM media per cortex. The cells were plated in a T-175 $cm^2$ culture flask coated with PDL (10 mg $mL^{-1}$ in MQ). The cells were incubated for 7 days at 37 °C and 5% $CO_2$ with the media changed twice per week. After 6 days in the culture flask, the cells were agitated on an orbital shaker (300 rpm) for 4–5 h at 37 °C and 5% $CO_2$. Then, the medium was changed. On day 7, the cells were again agitated for 2–3 h at 37 °C and 5% $CO_2$ to purify the astrocytes from the microglia cells.[26] After this procedure, the cells were replated for the different experiments, that is, the cell viability, the uptake of the HVs, the calcium imaging, and the immunostaining.

*Cell Viability—HVs*: The primary astrocytes were seeded in a 96-well plate with a cell density of around 45 000 cells per well and incubated for 7 days, after replating, at 37 °C and 5% $CO_2$ with the media changed twice per week. The fluorescently labeled HVs ($^{mix1}HV_0$, $^{mix1}HV_{CL\text{-}1}$, and $^{mix1}HV_{CL\text{-}2}$) were added on day 6 and the cell viability of the primary astrocytes was measured with the CCK-8 assay kit with the same procedure as described for the cell line.

*HV Uptake*: The primary astrocytes were seeded in a 24-well plate with a cell density of around 300 000 cells per well and incubated for 7 days, after replating, at 37 °C and 5% $CO_2$ with the media changed twice per week. 50 µL of the fluorescently labeled HVs ($^{mix1}HV_0$, $^{mix1}HV_{CL\text{-}1}$, and $^{mix1}HV_{CL\text{-}2}$) were added to the media for 48 h (after 24 h, the media was replaced with new media + 50 µL of HVs), 24 h, 6 h, and 3 h before measuring the uptake with of the HVs at day 7. The cells were washed twice with PBS. Then, 120 µL trypsin-EDTA was added to each well and incubated for 5 min at 37 °C and 5% $CO_2$. For neutralization, the cells were resuspended in 500 µL culture media. The cells were centrifuged for 5 min at 1500 rpm and the media was replaced with 500 µL 2% BSA in PBS. The uptake of the HVs was measured with the flow cytometer (BD Accuri C6 Plus) by using $\lambda_{ex} = 488$ nm and $\lambda_{em} = 520–550$ nm in the green channel and $\lambda_{em} = 565–605$ nm in the yellow channel. The fluorescence in each channel was analyzed by plotting the histogram for the green and yellow fluorescence followed by gating the cells into two populations. The first gate was created from the samples containing cells only. The second gate was for the cells with a fluorescence signal higher than the autofluorescence. The percentage of cells and the green and yellow CMF were found for each population individually.

The uptake of the HVs was also evaluated with CLSM. ≈1 500 000 primary astrocytes were seeded in a confocal dish (35 mm) and incubated for 7 days, after replating, with the media changed twice per week. On day 5, 50 µL of the fluorescently labeled HVs ($^{mix1}HV_0$, $^{mix1}HV_{CL\text{-}1}$, and $^{mix1}HV_{CL\text{-}2}$) were added to the primary astrocytes in 1.5 mL of DMEM media followed by incubation for 24 h at 37 °C and 5% $CO_2$. The media was then replaced by new DMEM media with 50 µL of fluorescently labeled HVs. The astrocytes were incubated for 24 h at 37 °C and 5% $CO_2$. The cells were washed twice with PBS and stained with 1 mL LysoTracker Deep Red diluted to 50 nM in pre-warmed media followed by 45 min incubation at 37 °C and 5% $CO_2$. The staining solution was replaced by 170 µL of PBS for storage. The cells were visualized using a Zeiss LSM710 confocal laser scanning microscope (Carl Zeiss, Germany) using a 40× oil objective. The lipids ($^{Rho}$PE) in the HVs were visualized using a $\lambda_{ex} = 572$ nm and $\lambda_{em} = 590$ nm, the $P1^{OG}$ in the HVs was visualized using a $\lambda_{ex} = 498$ nm and $\lambda_{em} = 526$ nm, and the lysosomes in the cells were visualized using a $\lambda_{ex} = 646$ nm and $\lambda_{em} = 664$ nm.

*Cell Viability—Paper Chips*: The sterile untreated or PDL-coated paper chips (paper chips 1 and 2) were added on top of 1 mL culture media in a 24-well plate. Different amounts (between 50 000 and 150 000 cells) of primary astrocytes were added to the hydrophilic central part of each paper chip and incubated for 14 days, after replating, at 37 °C and 5% $CO_2$. The culture media was changed once per week. The cell viability in the paper chips was visualized by CLSM using a LIVE/DEAD Viability/Cytotoxicity Kit. The papers were flipped and washed 2× with PBS after 14 days of incubation. 1 mL of staining solution containing ethidium homodimer-1 ($4 \times 10^{-6}$ M final concentration) and calcein-AM ($2 \times 10^{-6}$ M final concentration) in PBS was added to each well and incubated for 45 min at 37 °C and 5% $CO_2$. The cells were visualized with CLSM using a 20× or 10× objective. The live cells stained with calcein-AM were visualized using a $\lambda_{ex} = 493$ nm and $\lambda_{em} = 514$ nm and the dead cells stained with ethidium homodimer-1 were visualized using $\lambda_{ex} = 528$ nm and $\lambda_{em} = 617$ nm.

*Calcium Release—Paper Chip*: The primary astrocytes were seeded in paper chip 2 with a cell density of 150 000 cells per paper chip. The calcium signalling of the cells was measured with the Fluo-4 NW Calcium Assay Kit. The papers were washed 2× with PBS and incubated with Fluo-4 dye solution (2 µM) for 1 h. The cells were placed on a coverslip and 100 µL of PBS was added to the paper to avoid drying. ATP (100 µM) was added, and a time series was recorded with the CLSM using a 10× objective ($\lambda_{ex} = 494$ nm and $\lambda_{em} = 516$ nm).

*Immunostaining—Paper Chip*: 150 000 primary astrocytes were seeded in paper chip 2 on top of 1 mL of DMEM culture media in a 24-well plate and incubated for 14 days, after replating, at 37 °C and 5% $CO_2$ with the media changed once per week. The papers were washed quickly with PBS and 500 µL of 4% paraformaldehyde in PBS was added for fixation

followed by 15 min incubation at room temperature. The papers were washed with PBS for 3 × 10 min at room temperature (RT) followed by permeabilization with 500 µL TX (5% in PBS) for 30 min at RT. Again, the papers were washed with PBS for 3 × 10 min at RT. The cells were blocked with 10% FBS in PBS for 1 h at RT. The blocking solution was removed and 500 µL of the primary antibodies anti-GFAP (1:200 in PBS with 10% FBS) was added followed by incubation overnight at 4 °C. The next day, the papers were washed for 3 × 5 min with PBS. Then, 500 µL of the secondary antibody goat anti-mouse Alexa 488 (1:600 in PBS with 10% FBS) was added followed by incubation at RT for 20 min. The papers were washed twice with PBS for 10 min and then 500 µL Hoechst 33342 (1:200 in PBS) was incubated with the papers for 15 min at RT. The staining solution was removed, and the papers were washed with PBS. The cells were visualized with CLSM using a 20× and 40× objective.

*Uptake of HVs—Paper Chip*: 150 000 primary astrocytes were seeded in paper chip 2 on top of 1 mL of DMEM culture media in a 24-well plate and incubated for 14 days, after replating, at 37 °C and 5% $CO_2$ with the media changed once per week. 50 µL of the fluorescently labeled HVs ($^{mix1}HV_0$, $^{mix1}HV_{CL\text{-}1}$, and $^{mix1}HV_{CL\text{-}2}$) were added on top of the paper and the papers were incubated for 24 h at 37 °C and 5% $CO_2$. After the 24 h, another 50 µL of HVs were added on top of the paper followed by incubation for another 24 h at 37 °C and 5% $CO_2$. The papers were flipped and washed twice with PBS after which they were stained with 1 mL LysoTracker Deep Red staining solution (50 nM in pre-warmed media) followed by 45 min incubation at 37 °C and 5% $CO_2$. The cells in the paper chips were visualized with CLSM using a 20× objective. The lipids ($^{Rho}$PE) in the HVs were visualized using a $\lambda_{ex}$ = 572 nm and $\lambda_{em}$ = 590 nm, the $P1^{OG}$ in the HVs was visualized using a $\lambda_{ex}$ = 498 nm and $\lambda_{em}$ = 526 nm, and the lysosomes in the cells were visualized using a $\lambda_{ex}$ = 646 nm and $\lambda_{em}$ = 664 nm.

*Statistical Analysis*: All experiments were performed with at least two technical repeats averaged to one independent repeat. All experiments were performed with $n$ = 3, indicating three independent repeats with different batches of HVs and different passages of cells (for the cell line). All data were presented as mean values ± SD for $n$ = 3. The cell viability data were normalized to the untreated cells in all cases. The data were statistically analyzed using one-way ANOVA followed by a Tukey's multiple comparison test ($^*p \leq 0.05$) by using Prism. The flow cytometry data was analyzed using floreada.io. The histograms from the green and yellow channels were obtained, and the counts were gated into two populations (a negative and a positive population). The percentage of cells in each population and the CMF were determined with floreado.io and presented as mean values ± SD. The statistical significance was found using one-way ANOVA followed by a Tukey's multiple comparison test ($^*p \leq 0.05$) by using Prism. The calcium signalling assays were analyzed in more detail by determining the fluorescent intensity of 4–5 representative cells over time using the Fiji plugin Time Series Analyzer V3. The background fluorescence in each well was measured for 2 min before the addition of ATP and histamine for the calcium signalling measurements with the plate reader. The background fluorescence in each well was averaged over the measurement time and subtracted from the fluorescence in each well in the assay before averaging the independent repeats.

The size distribution of the HVs was presented as histograms and fitted to a log normal distribution. The mean sizes were obtained from fitting with MATLAB. Two independent repeats of the HV permeability assay were performed. The data was normalized by dividing the maximum value and the linear decay of each of the repeats was fitted to a linear regression to calculate the slope. The statistical significance was determined using one-way ANOVA followed by a Tukey's multiple comparison test ($^*p \leq 0.05$) by using Origin.

## Supporting Information

Supporting Information is available from the Wiley Online Library or from the author.

## Acknowledgements

This project was supported by the European Research Council (ERC) under the European Union's Horizon 2020 research and innovation programme (grant agreement No. 818890), the Lundbeck Foundation (R346-2020-1617), and the Carlsberg Foundation (CF 20–0418). The HRM Queen Margrethe II's travel grant (C.A.M.) is acknowledged for support. The authors thank Dr. Miguel Alexandre Ramos Docampo for taking the SEM images. The authors acknowledge the Instituto de Medicina Molecular João Lobo Antunes Bioimaging and Flow Cytometry Units for their support.

## Conflict of Interest

The authors declare no conflict of interest.

## Data Availability Statement

The raw/processed data required to reproduce these findings are available to download from http://sciencedata.dk/shared/4bf96831e44855810e56cb41ccbf45f0.

## Keywords

astrocytes, calcium signalling, hybrid vesicles, paper-based chips

Received: July 22, 2022
Revised: October 3, 2022
Published online: November 3, 2022

[1] C. Escartin, E. Galea, A. Lakatos, J. P. O'Callaghan, G. C. Petzold, A. Serrano-Pozo, C. Steinhäuser, A. Volterra, G. Carmignoto, A. Agarwal, N. J. Allen, A. Araque, L. Barbeito, A. Barzilai, D. E. Bergles, G. Bonvento, A. M. Butt, W.-T. Chen, M. Cohen-Salmon, C. Cunningham, B. Deneen, B. De Strooper, B. Díaz-Castro, C. Farina, M. Freeman, V. Gallo, J. E. Goldman, S. A. Goldman, M. Götz, A. Gutiérrez, et al., *Nat. Neurosci.* **2021**, *24*, 312.

[2] A. Armada-Moreira, J. I. Gomes, C. C. Pina, O. K. Savchak, J. Gonçalves-Ribeiro, N. Rei, S. Pinto, T. P. Morais, R. S. Martins, F. F. Ribeiro, A. M. Sebastião, V. Crunelli, S. H. Vaz, *Front. Cell. Neurosci.* **2020**, *14*, 90.

[3] A. Araque, G. Carmignoto, P. G. Haydon, S. H. R. Oliet, R. Robitaille, A. Volterra, *Neuron* **2014**, *81*, 728.

[4] J. I. Alvarez, T. Katayama, A. Prat, *Glia* **2013**, *61*, 1939.

[5] a) S. H. Vaz, S. Pinto, A. M. Sebastião, D. Brites, in *Amyotrophic Lateral Sclerosis* (Ed: T. Araki), Exon Publications, Brisbane **2021**; b) M. Barbosa, C. Gomes, C. Sequeira, J. Gonçalves-Ribeiro, C. C. Pina, L. A. Carvalho, R. Moreira, S. H. Vaz, A. R. Vaz, D. Brites, *Front. Cell Dev. Biol.* **2021**, *9*, 634355.

[6] a) Y. Cai, X. Chen, J. Si, X. Mou, X. Dong, *Small* **2021**, *17*, 2103072; b) C.-L. Chiang, M.-H. Cheng, C.-H. Lin, *Nanomaterials* **2021**, *11*, 1727; c) S. Mignani, X. Shi, K. Guidolin, G. Zheng, A. Karpus, J.-P. Majoral, *J. Controlled Release* **2021**, *337*, 356; d) V. Kumar, M. Rahman, P. Gahtori, F. Al-Abbasi, F. Anwar, H. S. Kim, *Expert. Opin. Drug Delivery* **2021**, *18*, 673.

[7] H. H. Chowdhury, S. R. Cerqueira, N. Sousa, J. M. Oliveira, R. L. Reis, R. Zorec, *Biomater. Sci.* **2018**, *6*, 388.

[8] S. Papa, V. Veneruso, E. Mauri, G. Cremonesi, X. Mingaj, A. Mariani, M. De Paola, A. Rossetti, A. Sacchetti, F. Rossi, G. Forloni, P. Veglianese, *J. Controlled Release* **2021**, *330*, 218.

[9] a) M. Mohammadi, S. Taghavi, K. Abnous, S. M. Taghdisi, M. Ramezani, M. Alibolandi, *Adv. Funct. Mater.* **2018**, *28*, 1802136; b) M. Schulz, W. H. Binder, *Macromol. Rapid Commun.* **2015**, *36*, 2031; c) M. Schulz, A. Olubummo, W. H. Binder, *Soft Matter* **2012**, *8*, 4849.
[10] S. Li, X. Xie, W. Wang, S. Jiang, W. Mei, Y. Zhang, S. Liu, X. Yu, *Nanoscale* **2022**, *14*, 2277.
[11] a) B. S. Esposto, P. Jauregi, D. R. Tapia-Blácido, M. Martelli-Tosi, *Trends Food Sci. Technol.* **2021**, *108*, 40; b) C. Tan, J. Wang, B. Sun, *Biotechnol. Adv.* **2021**, *48*, 107727.
[12] a) M. Talelli, M. Barz, C. J. F. Rijcken, F. Kiessling, W. E. Hennink, T. Lammers, *Nano Today* **2015**, *10*, 93; b) M. Lin, Y. Dai, F. Xia, X. Zhang, *Mater. Sci. Eng., C* **2021**, *119*, 111626.
[13] S. Varlas, J. C. Foster, P. G. Georgiou, R. Keogh, J. T. Husband, D. S. Williams, R. K. O'Reilly, *Nanoscale* **2019**, *11*, 12643.
[14] C. Ade, X. Qian, E. Brodszkij, P. De Dios Andres, J. Spanjers, I. N. Westensee, B. Städler, *Biomacromolecules* **2022**, *23*, 1052.
[15] P. De Dios Andres, I. N. Westensee, E. Brodszkij, M. A. Ramos-Docampo, N. Gal, B. Städler, *Biomacromolecules* **2021**, *22*, 3860.
[16] a) P. J. Magistretti, L. Pellerin, D. L. Rothman, R. G. Shulman, *Science* **1999**, *283*, 496; b) P. J. Magistretti, L. Pellerin, *Philos. Trans. R. Soc., B* **1999**, *354*, 1155; c) G. A. Dienel, L. Hertz, *J. Neurosci. Res.* **2001**, *66*, 824.
[17] M. Y. Batiuk, A. Martirosyan, J. Wahis, F. de Vin, C. Marneffe, C. Kusserow, J. Koeppen, J. F. Viana, J. F. Oliveira, T. Voet, C. P. Ponting, T. G. Belgard, M. G. Holt, *Nat. Commun.* **2020**, *11*, 1220.
[18] L. Wang, C. Xu, Y. Zhu, Y. Yu, N. Sun, X. Zhang, K. Feng, J. Qin, *Lab Chip* **2015**, *15*, 4283.
[19] H.-J. Park, S. J. Yu, K. Yang, Y. Jin, A.-N. Cho, J. Kim, B. Lee, H. S. Yang, S. G. Im, S.-W. Cho, *Biomaterials* **2014**, *35*, 9811.
[20] a) B. Esteban-Fernández de Ávila, P. Angsantikul, J. Li, W. Gao, L. Zhang, J. Wang, *Adv. Funct. Mater.* **2018**, *28*, 1705640; b) T. Agarwal, M. R. Borrelli, P. Makvandi, M. Ashrafizadeh, T. K. Maiti, *ACS Appl. Bio Mater.* **2020**, *3*, 3956.
[21] M. J. Aebersold, G. Thompson-Steckel, A. Joutang, M. Schneider, C. Burchert, C. Forró, S. Weydert, H. Han, J. Vörös, *Front. Neurosci.* **2018**, *12*, 94.
[22] P. de Dios Andres, B. Städler, *Small* **2022**, 2201251.
[23] a) L. R. James, S. Andrews, S. Walker, P. R. de Sousa, A. Ray, N. A. Russell, T. C. Bellamy, *PLoS One* **2011**, *6*, e26889; b) M. Morita, C. Higuchi, T. Moto, N. Kozuka, J. Susuki, R. Itofusa, J. Yamashita, Y. Kudo, *J. Neurosci.* **2003**, *23*, 10944.
[24] T. P. Morais, D. Coelho, S. H. Vaz, A. M. Sebastião, C. A. Valente, *Front. Mol. Neurosci.* **2018**, *10*, 444.
[25] S. H. Vaz, T. N. Jørgensen, S. Cristóvão-Ferreira, S. Duflot, J. A. Ribeiro, U. Gether, A. M. Sebastião, *J. Biol. Chem.* **2011**, *286*, 40464.
[26] F. Du, Z. M. Qian, L. Zhu, X. M. Wu, C. Qian, R. Chan, Y. Ke, *J. Cell. Biochem.* **2010**, *109*, 30.